OFFICE OF SCIENTIFIC RESEARCH AND DEVELOPMENT
NATIONAL DEFENSE RESEARCH COMMITTEE
DIVISION SIX — SECTION 6.1

# FORCE AND CAVITATION CHARACTERISTICS OF THE NACA 4412 HYDROFOIL

BY

ROBERT T. KNAPP
OFFICIAL INVESTIGATOR

THE HIGH SPEED WATER TUNNEL
AT THE
CALIFORNIA INSTITUTE OF TECHNOLOGY
HYDRAULIC MACHINERY LABORATORY
PASADENA, CALIFORNIA

Section No. 6.1-sr207-1273

HML No. ND-19

Report Prepared by
James W. Daily
Hydraulic Engineer

June 10, 1944

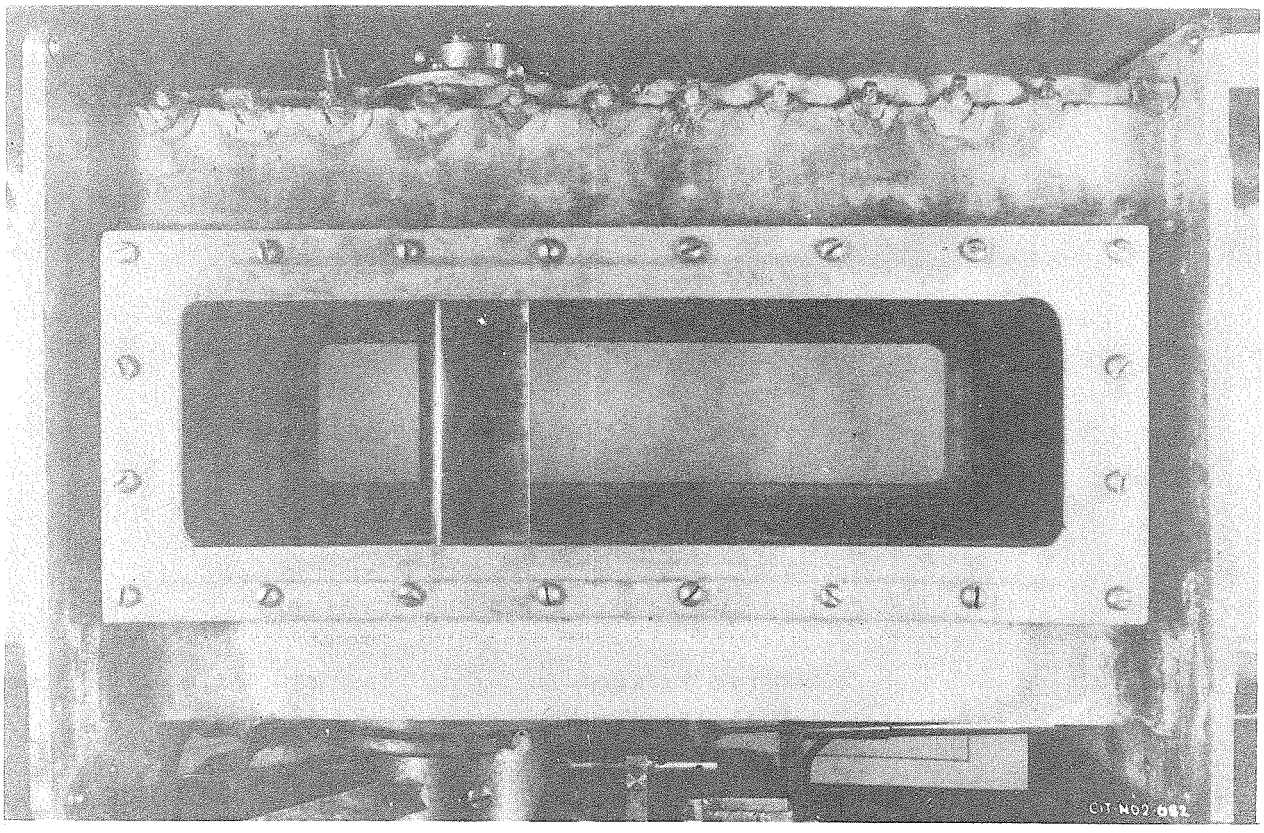

THE NACA 4412 HYDROFOIL
AS VIEWED THROUGH THE TRANSPARENT WINDOWS OF THE
WATER TUNNEL WORKING SECTION

# ABSTRACT

The High Speed Water Tunnel is operated by the California Institute of Technology under Contract OEMsr-207 with the OSRD and is sponsored by Division 6, Section 6.1 of the NDRC. The investigations reported here were made at the request of the United States Navy Department, David Taylor Model Basin, as authorized by a letter of January 17, 1944, from Dr. E. H. Colpitts, Chief of Section 6.1, NDRC.

This report covers Water Tunnel tests of a "two-dimensional" installation of a 3" chord, 10" span section of the NACA 4412 profile. The tests included measurements during cavitation-free operation of the hydrodynamic forces and moments as functions of the angle of attack and velocity of flow, and observations under cavitating conditions of the inception and growth of cavitation for different angles of attack as functions of the cavitation parameter, K. The results are compared with existing information on this hydrofoil from other sources and the Water Tunnel test methods for obtaining the hydrodynamic characteristics of hydrofoils are discussed. The main findings are as follows:

1. Water Tunnel testing provides a very satisfactory method of observing and measuring cavitation characteristics of hydrofoils as well as non-cavitating characteristics, all with a single test installation.

2. Photographs of cavitation and the simultaneous pressure and velocity measurements illustrate:

   a) The acceleration of inception of cavitation by increase in velocity or by decrease in pressure (either one of which causes the cavitation parameter, K, to become smaller), and by increase in angle of attack. The results are summarized conveniently in the form of curves of submergence required to avoid cavitation for different velocities and attack angles.

   b) The inception, first on one face and then on the other face of the hydrofoil, as the cavitation parameter is reduced.

   c) The change in magnitude and the character of the cavitation bubble with angle of attack and with cavitation parameter.

   d) The effect of small surface irregularities or adhesion of foreign material to the leading edge of the hydrofoil in accelerating inception of cavitation.

3. With the "two-dimensional" test installations the infinite aspect ratio or "section" characteristics can be approximated without data correction of any kind. This is in contrast with the normal type of installation with three-dimensional flow about short spans which require elaborate corrections to obtain infinite aspect ratio characteristics.

4. Evaluation of possible errors indicates that the accuracy of these data is good in the low-lift range of normal hydrofoil applications. At high lifts (large attack angles) the absolute accuracy is reduced but the good comparative results should still obtained.

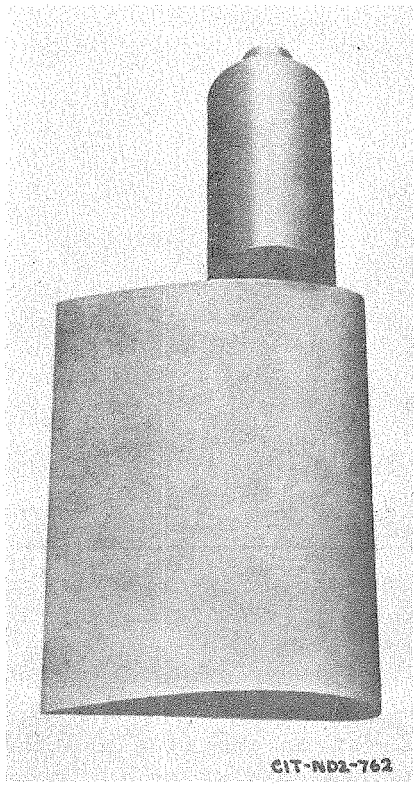


FIGURE 1

NACA 4412

HYDROFOIL TEST SPAN

# WATER TUNNEL MEASUREMENTS OF THE INFINITE ASPECT RATIO CHARACTERISTICS AND CAVITATION CHARACTERISTICS OF THE NACA 4412 HYDROFOIL SECTION

## I. PURPOSE AND SCOPE OF THE INVESTIGATION

This report covers Water Tunnel measurements of the infinite aspect ratio characteristics and cavitation characteristics of a hydrofoil section. The profile tested is identical to the 4412 airfoil section of the National Advisory Committee for Aeronautics and is called the NACA 4412 hydrofoil in this report. Measurements and observations include lift, drag, and pitching moment and the inception and development of cavitation as functions of the angle of attack, velocity and pressure of the flow. The purpose of this report is to present these measurements of the characteristics of this section in water, to compare the results with other available information on this shape, and to evaluate the Water Tunnel method for obtaining the complete hydrodynamic characteristics of hydrofoils.

## II. DESCRIPTION OF INSTALLATION AND TESTS

The tests described in this report were made in the High Speed Water Tunnel at the California Institute of Technology.(1) For the experiments, solid stainless steel test sections of the NACA 4412 hydrofoil with a chord length of 3 inches were supplied the laboratory by the David Taylor Model Basin. The 4412 profile is one of the four digit series of shapes of the National Advisory Committee for Aeronautics described in References (2), (3), (4), and (5). It is a 4% cambered section with a 12% thickness ratio. Dimensions of the profile are tabulated in Appendix C. Figures 1, 2, and 3 are photographs of the test units.

For these tests a special arrangement of the Water Tunnel working section was used where a 3.33 aspect ratio hydrofoil test unit spanned a 10" gap between parallel tunnel walls. This installation, which gave approximately two-dimensional flow, is described in Appendix A. Two different hydrofoil installations were used, permitting measurements of the hydrodynamic forces and moments acting on the complete 10" span or on only one-half the span. The latter was obtained by splitting the hydrofoil at the tunnel center line and supporting one-half independently of the

(1) Figures in parentheses refer to references in Appendix D

tunnel balance. For measurements at angles of attack both halves were rotated through the same angle. Figure 2 shows the test unit used for the full-span measurements and Figure 3 shows the two semispans used for the latter measurements. Details of the two installations are described in Appendix A.

Two types of experiments were made. The first was the determination of the hydrodynamic lift, drag, and pitching moment as functions of the angle of attack for cavitation-free operation at Reynolds numbers of from 287,000 to 903,000. The second was the observation of the inception and growth of cavitation at different angles of attack as functions of velocity and pressure. The effect of cavitation on the lift and drag was investigated qualitatively but detailed investigations were postponed because of the limited time available for the tests.

## III. INFINITE ASPECT RATIO CHARACTERISTICS OF THE NACA 4412 HYDROFOIL

Because of the two-dimensional character of the Water Tunnel test installation, the measured hydrodynamic forces and moments approximate the characteristics of a hydrofoil section with infinite aspect ratio. Infinite aspect ratio characteristics differ from those obtained by tests of a finite span airfoil or hydrofoil because of the occurrence for the finite span of the so-called "induced" effects.* These effects, which arise because of the large "leakage" of fluid at the tips of the foil from the high pressure bottom surface to low pressure top surface, reduce the lift and increase the drag at given angles of attack. The magnitude of the effects is different for changing aspect ratios, plan form, and twist of the section. Because of the absence of these secondary influences, infinite aspect ratio results are also called "section characteristics,"** denoting that they represent the basic behavior of the foil's profile shape independent of aspect ratio or other geometrical configurations. Data in this form is particularly useful to the designer of wings, propeller blades, or other lifting or pumping devices. Several methods have been developed for converting section characteristic data into the performance of finite span units with either uniform or varying sections. Some of these are reviewed in References (7), (8), and (9).

### CHARACTERISTICS FROM WATER TUNNEL MEASUREMENTS

The hydrodynamic characteristics of the 4412 hydrofoil as measured in the High Speed Water Tunnel are shown in Figures 4, 5, and 6. These data are derived directly from the Water Tunnel measurements without corrections of any kind. Definitions of the

*For a discussion of induced effects on airfoils, see References (6) and (7)

**The nomenclature and symbols used in this report and defined in Appendix B follow closely those employed in the several N.A.C.A. reports referred to throughout the text

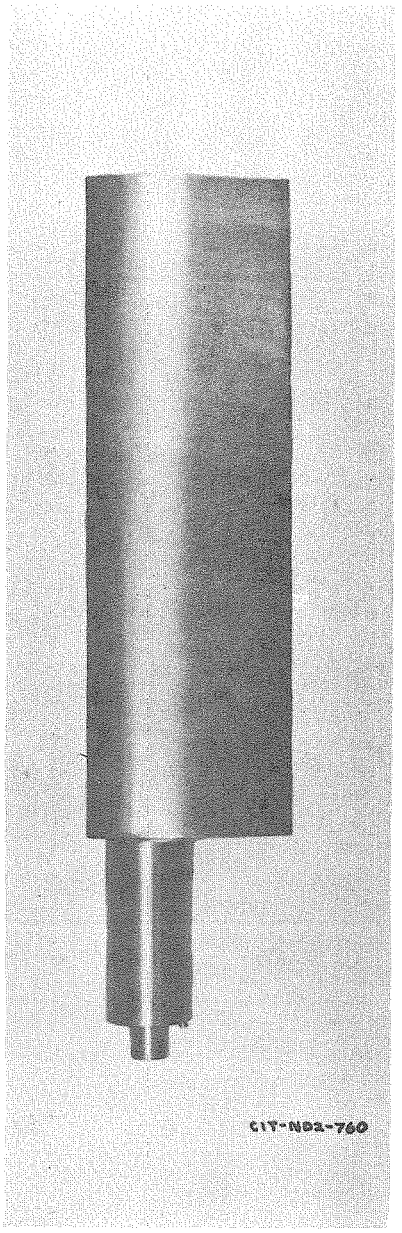


FIGURE 2

FULL 10"
SPAN TEST SECTION

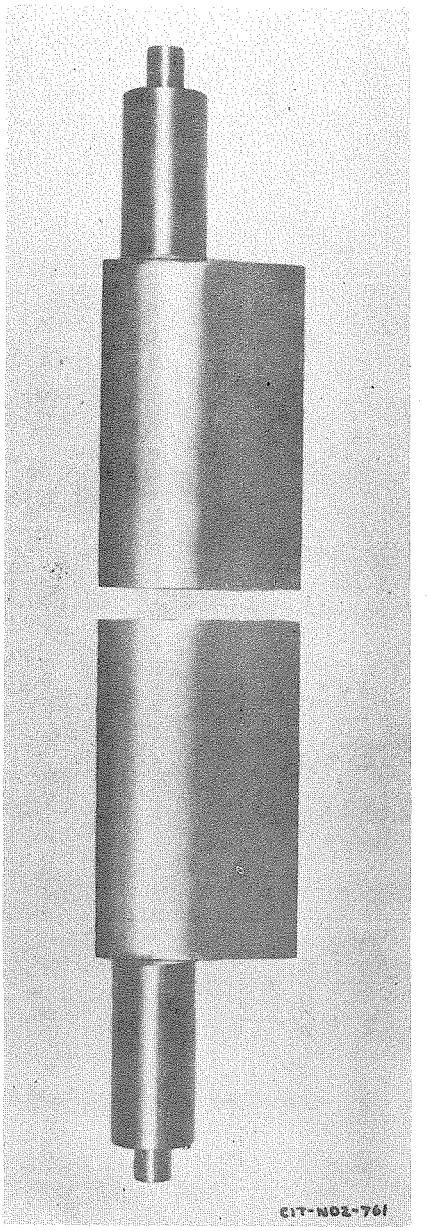


FIGURE 3

UPPER AND LOWER
SEMISPAN TEST SECTIONS

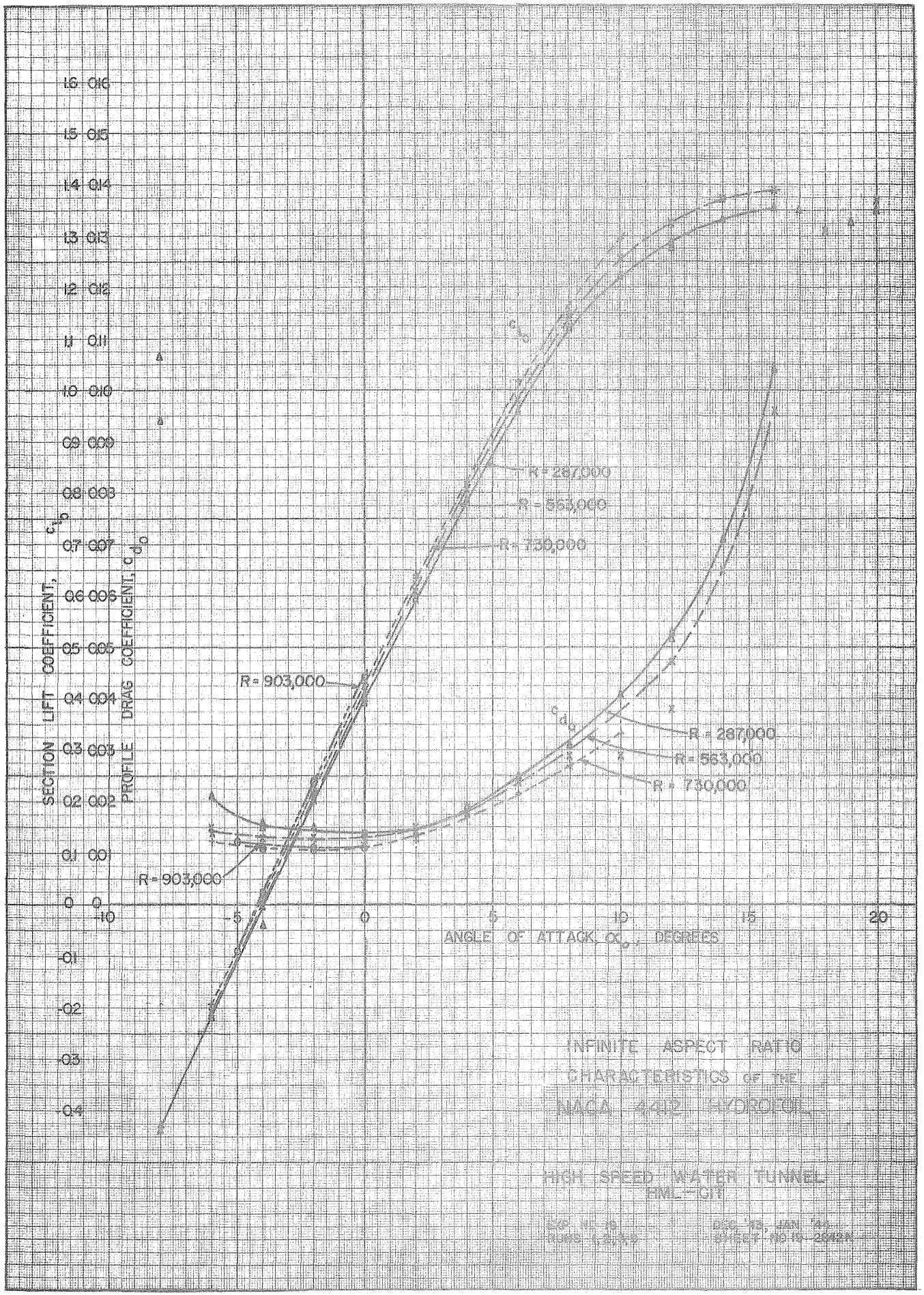
SECTION LIFT COEFFICIENT, $c_{l_o}$
PROFILE DRAG COEFFICIENT, $c_{d_o}$
ANGLE OF ATTACK, $\alpha_{o_f}$, DEGREES
$c_{l_o}$
$c_{d_o}$
R = 287,000
R = 563,000
R = 730,000
R = 903,000
INFINITE ASPECT RATIO
CHARACTERISTICS OF THE
NACA 442 HYDROFOIL
HIGH SPEED WATER TUNNEL
EML - GIT

FIGURE 4

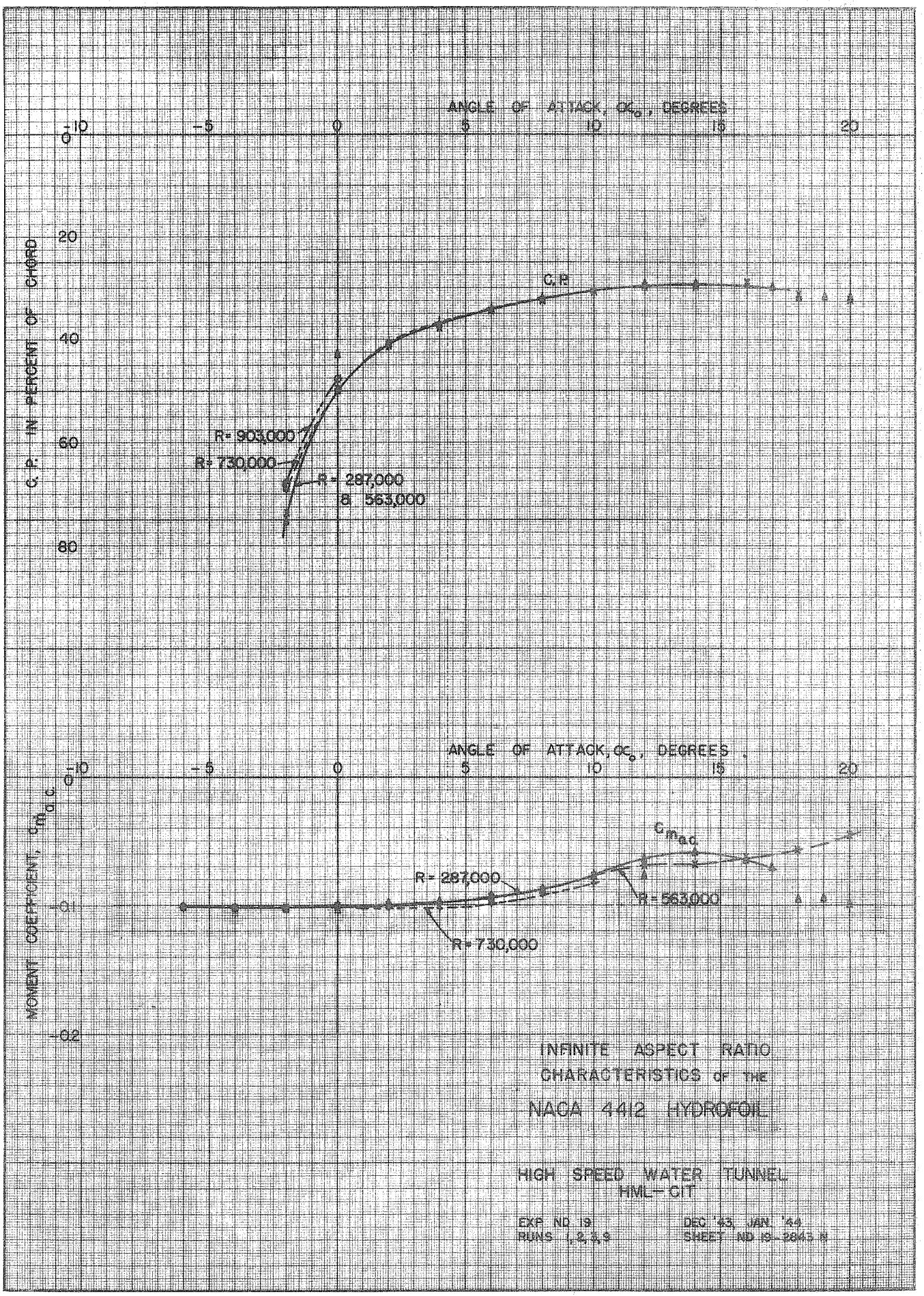
ANGLE OF ATTACK, $\alpha_{c_0}$, DEGREES
-10
-5
0
5
10
15
20
C. P. IN PERCENT OF CHORD
0
20
40
60
80
C.P.
R= 903,000
R= 730,000
R= 287,000
& 563,000
ANGLE OF ATTACK, $\alpha_{c_0}$, DEGREES
MOMENT COEFFICIENT, $C_{m_{a.c.}}$
-01
-02
$C_{m_{a.c.}}$
R= 287,000
R= 563,000
R= 730,000
INFINITE ASPECT RATIO
CHARACTERISTICS OF THE
NACA 4412 HYDROFOIL
HIGH SPEED WATER TUNNEL
HML- CIT
EXP. NO. 19
RUNS 1, 2, 3, 9
DEC '43, JAN. '44
SHEET NO 19-2843 R

FIGURE 5

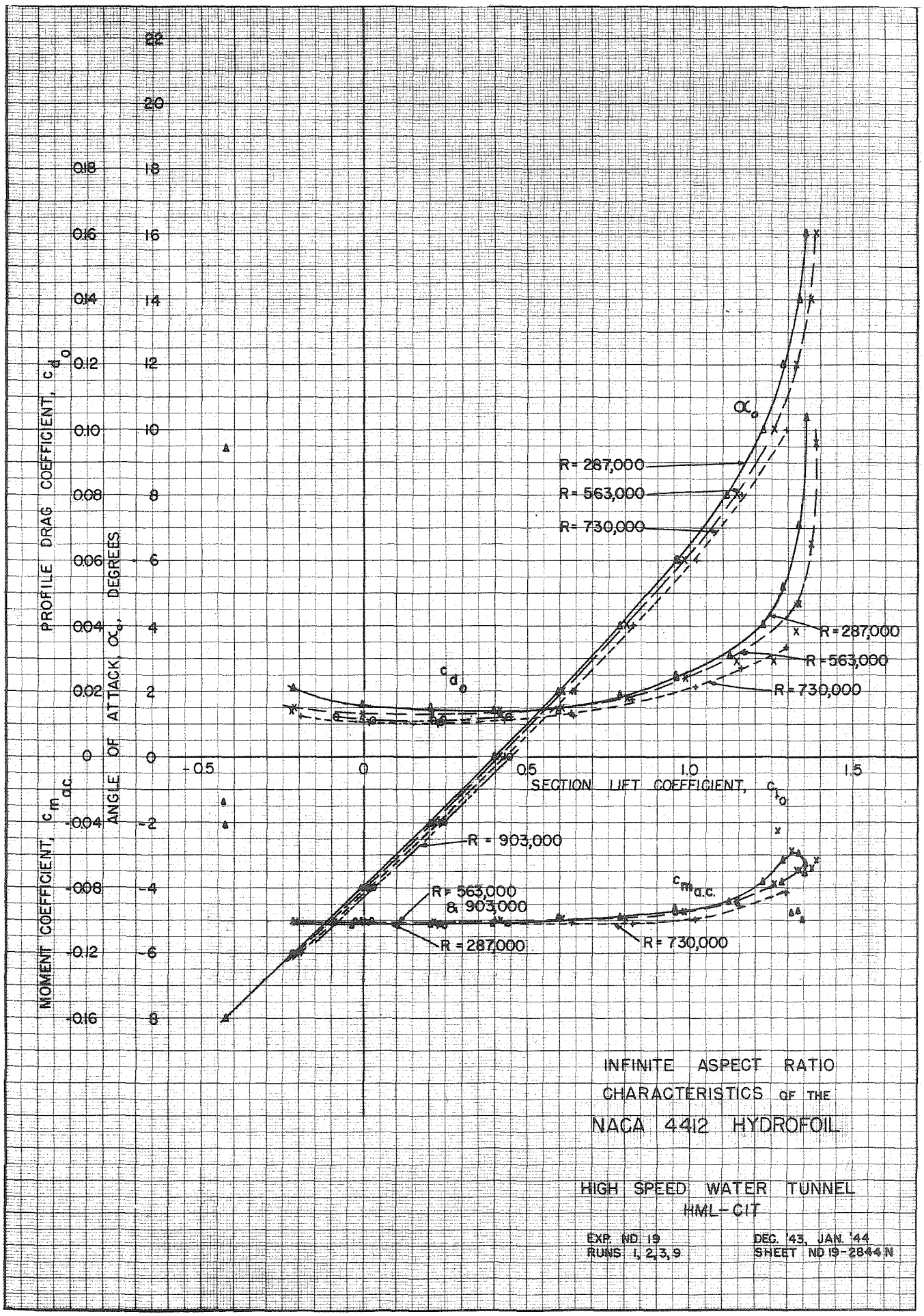
PROFILE DRAG COEFFICIENT, $c_{d_0}$
ANGLE OF ATTACK, $\alpha_o$, DEGREES
MOMENT COEFFICIENT, $c_{m_{a.c.}}$
SECTION LIFT COEFFICIENT, $c_{l_0}$
$\alpha_o$
$c_{d_0}$
$c_{m_{a.c.}}$
R = 287,000
R = 563,000
R = 730,000
R = 903,000
R = 563,000 & 903,000
INFINITE ASPECT RATIO
CHARACTERISTICS OF THE
NACA 4412 HYDROFOIL
HIGH SPEED WATER TUNNEL
HML-CIT
EXP. ND 19
RUNS 1, 2, 3, 9
DEC. '43, JAN. '44
SHEET ND 19-2844 N



FIGURE 6

terms and symbols used are given in Appendix B. Figures 4 and 5 show lift and drag coefficients, pitching moment coefficient, and center of pressure in per cent of the airfoil chord as functions of the angle of attack. Figure 6 is a diagram showing angle of attack and drag and pitching moment coefficients as functions of the lift coefficient. Four tests are shown in each diagram for the Reynolds number range of 287,000 to 903,000. These tests were all made with the split-span installation permitting measurement of the forces on only one-half the total span. Data could not be taken up to the maximum lift at all test Reynolds numbers because of the excessive magnitude of the forces developed. Only for the two lower Reynolds numbers was the complete behavior obtained. Data obtained with the full-span installation were limited to the lower Reynolds number range, and since they gave similar results, they were not included in these diagrams. The magnitudes of the important characteristics for both the semispan and full-span installations are listed for each Reynolds number in Table I.

The curves show certain consistent changes in performance with Reynolds number. The slope of the lift curve in Figure 4 becomes steeper with increasing R and the maximum lift coefficient becomes larger. The attack angle for zero lift decreases slightly (increases negatively) and the profile drag tends to become smaller. In Figure 5 the pitching moment coefficient is referred to the aerodynamic center, a point in the airfoil about which the pitching moment is essentially independent of angle of attack or lift for a wide range. In this figure the moment coefficient is nearly constant up to about $5^{\circ}$, and within 15% of a constant value up to $8^{\circ}$. Furthermore, all runs show nearly the same magnitude for $c_{m_{a.c.}}$. The center of pressure, also shown on Figure 5, is nearly independent of Reynolds number, the deviations from the mean curve occurring near zero attack angle where accuracy in calculating the C.P. position is low.

The same information is shown in the diagram of Figure 6 where the lift coefficient $c_{l_o}$ is considered as the independent variable instead of $\alpha_o$.

## DEVIATIONS FROM TRUE INFINITE ASPECT RATIO CHARACTERISTICS

The only deviations of these results from real two-dimensional characteristics will be caused first, by variation of velocity along the span of the hydrofoil from the center of the working section on through the boundary layer to the tunnel wall; second, by flow through the clearance spaces between the ends of the foil and the tunnel walls or between the two halves of the split-span installation; and third, by interference from the tunnel walls.

Deviations from a uniform velocity distribution will tend to make all the coefficients numerically high. However, as shown in Figure A-5 of Appendix A, the hydrofoil test unit was located in the measuring section about one "diameter" downstream from the

final contraction of the flow. With so short a distance the boundary layer growth should be small. Consequently, most of the hydrofoil span should experience the full velocity of the central uniform portion of the velocity profile, and the resulting hydrodynamic forces and moments should be reasonably accurate.

The principal effect of "leakage" flow through the gaps between the tunnel walls and the hydrofoil and between the ends of the split hydrofoil will be to reduce the actual angle of attack at the hydrofoil for high lifts. All clearance gaps were held to approximately 0.005" so that the resistance to flow through them was high. At small angles of attack the influence on the measured forces and moments should be negligible. However, as the lift increases, enough leakage flow may occur to reduce the maximum lift coefficient appreciably. This is an error in lift and moment that would be reduced by using end plates set into the tunnel walls instead of clearance gaps. However, it is not felt to be as satisfactory an arrangement for measuring drags. It should be emphasized that the clearance gap effect is important so that good control of the gap is essential. Changing the gap clearance from 0.023" to 0.005" causes about an 8% decrease in drag. If it is assumed that the error introduced by leakage through the clearance gap is proportional to the leakage (which in turn is proportional to the gap for laminar flow through small clearances), the maximum error to be expected with 0.005" gap is less than 2%. It is more likely that the error increases at a greater rate as the gap is enlarged so that the error at 0.005" is even less. Changing the gap clearance from 0.023" to 0.005" causes about a 4% increase in lift, but has no appreciable effect to the moment. By the reasoning just outlined, the error in lift at 0.005" is also probably negligible.

Tunnel wall interference changes the streamline pattern around the hydrofoil from that experienced in a free stream. The walls parallel to the pitching axis are important for two-dimensional flow and it was with this in mind that the maximum dimension normal to the hydrofoil axis was held to the full 14", as shown in Figure A-5 of Appendix A. Wall interference, including the so-called "blocking" or actual restriction of the passage by the test unit itself, is negligible at low lift (small angles of attack). At high lifts it is much more important and should show greatest effect at the maximum lift. The actual magnitude of the wall interference has not been evaluated.

To summarize, it appears that these tests give accurate results in the low-lift range, the normal range of application for hydrofoils. At high lifts the accuracy is lower but good comparative results are still obtainable.

## THEORETICAL CHARACTERISTICS

It is of interest to compare these Water Tunnel measurements with the characteristics that can be calculated from theoretical consideration of an infinite span section in a nonviscous fluid.[7] Such a treatment gives, for small angles of attack, a lift coefficient proportional to the angle of attack, an attack angle for zero lift proportional to the amount of camber, and a moment coefficient constant about the quarter chord point. These relationships are:

Lift coefficient $= c_{l_o} = 2\pi \left(1 + 0.77 \frac{\text{thickness}}{\text{chord}}\right) \frac{(\alpha_o - \alpha_{l_o})}{57.3}$

Zero lift angle $= \alpha_{l_o} = .2 \frac{\text{camber}}{\text{chord}} \times 57.3$

Slope of lift curve $= a_o = 2\pi \left(1 + 0.77 \frac{\text{thickness}}{\text{chord}}\right) \frac{1}{57.3}$

Pitching moment coefficient $= c_{m_{a.c.}} = \frac{\pi}{2} \left(1 + 0.77 \frac{\text{thickness}}{\text{chord}}\right) \frac{\alpha_{l_o}}{57.3}$

For the 4412 hydrofoil the numerical values are:

$c_{l_o} = 0.120 (\alpha_o - \alpha_{l_o})$

$\alpha_{l_o} = -4.6^\circ$

$a_o = 0.120$ (per degree)

$c_{m_{a.c.}} = -0.137$

Since frictionless flow is assumed, the above are independent of Reynolds number. Also, because of the zero friction assumption, this treatment gives zero drag and gives no information about the maximum lift coefficient to be obtained. Comparison in Table I of the theoretical values with the measured values shows that the former are slightly higher (numerically) in each case.

## CHARACTERISTICS FROM NACA WIND TUNNEL MEASUREMENTS

The 4412 profile has been thoroughly tested in the NACA Variable Density Wind Tunnel and its characteristics reported in a series of technical reports.[2], [3], [4], [5] These measurements were made on finite rectangular span sections having an

RESTRICTED

TABLE I

PRINCIPAL SECTION CHARACTERISTICS OF THE NACA 4412 HYDROFOIL FROM TWO-DIMENSIONAL TESTS IN WATER TUNNEL

| | Test Reynolds Number | Attack Angle for no lift $\alpha_{l_o}$ (deg) | Lift Curve Slope $a_o$ (per deg) | Max. Lift Coefficient $c_{l_{max}}$ | Min. Drag Coefficient $c_{d_{o\ min}}$ | Pitching Moment $c_{m_{a.c.}}$ | Aerodynamic Center Ahead of c/4 (% c) | Aerodynamic Center Above Chord (% c) |
|---|---|---|---|---|---|---|---|---|
| Semispan Installation | 287,000 | -3.95 | 0.098 | 1.36 | 0.014 | -0.102 | 5.47 | -0.26 |
| | 563,000 | -4.05 | 0.102 | 1.39 | 0.013 | -0.101 | 4.92 | -4.52 |
| | 730,000 | -4.15 | 0.104 | | 0.0105 | -0.102 | 5.53 | -3.84 |
| | 903,000 | -4.25 | 0.106 | | 0.011 | -0.101 | 5.39 | 1.68 |
| Full-span Installation | 299,000 | -4 (approx)* | 0.098 | 1.38 | 0.014 | -0.100 | 5.12 | -0.38 |
| | 388,000 | -4 (approx)* | 0.101 | | 0.014 | -0.102 | 5.12 | -0.39 |
| Theoretical Values for Infinite Aspect Ratio | | -4.58 | 0.120 | | | -0.137 | 0 | 0 |

*These values for $\alpha_{l_o}$ are obtained after correction for error in initial alignment of hydrofoil chord with tunnel axis

TABLE II

PRINCIPAL SECTION CHARACTERISTICS OF THE NACA HYDROFOIL
FROM WIND TUNNEL TESTS OF RECTANGULAR AIRFOILS
WITH ASPECT RATIO = SIX*

| Test Reynolds Number | Attack Angle for no lift $\alpha_{l_o}$ (deg) | Lift Curve Slope $a_o$ (per deg) | Max. Lift Coefficient $c_{l_{max}}$ | Min. Drag Coefficient $c_{d_{o\ min}}$ | Pitching Moment $c_{m_{a.c.}}$ | Aerodynamic Center Ahead of c/4 (% c) | Aerodynamic Center Above Chord (% c) |
|---|---|---|---|---|---|---|---|
| 331,000 | -4.35 | 0.094 | 1.27 | 0.011 | -0.096 | 1.1 | -8.0 |
| 638,000 | -4.25 | 0.094 | 1.36 | 0.012 | -0.094 | 1.0 | -1.0 |

*Wind Tunnel data were taken from Figure 7, Reference 5, and corrected by the methods outlined on Pages 17 and 18 of that reference to give so-called "second approximation" characteristics.





RESTRICTED

aspect ratio of six. These data were then corrected for induced velocity effects, for Wind Tunnel wall interference, and for support interference effects to get the infinite aspect ratio or section characteristics. In Figures 7 and 8, two of the Water Tunnel tests are compared with two of the Wind Tunnel tests for comparable Reynolds numbers. The Wind Tunnel data are taken from Reference (5), and represent approximate section characteristics* at the test Reynolds number. All corrections to infinite aspect ratio are included except the effect of support interference on drag[6] and certain secondary effects of variations in $c_l$ and $c_{d_o}$ along the finite test span at high lifts. They are not corrected for turbulence or scale effects and should not be confused with final characteristics presented in References (5) and (6) which have been extrapolated to full-scale aircraft flight Reynolds numbers. In Table II, Page 11, the principal characteristics from the Wind Tunnel tests for these two Reynolds numbers and for several others are listed for comparison with the Water Tunnel values given in Table I. Both the figures and tabulations show some differences between the two sets of measurements. The angles for zero lift are comparable while the minimum drag coefficient, the slope of the lift curve, and the moment coefficient are all about 10% lower in the case of Wind Tunnel measurements. The latter two represent a more marked deviation from the theoretical values than shown by the Water Tunnel characteristics. The Wind Tunnel minimum drag coefficients are comparable at the higher Reynolds number but differ considerably at the lower R values. The maximum lift coefficient is higher for the Water Tunnel tests.

It is seen that the Water Tunnel results are as good or better than the corresponding Wind Tunnel data. Furthermore, they are obtained directly from tunnel measurements without corrections of any kind, whereas the finite span tests must be treated elaborately to obtain approximate infinite aspect ratio characteristics. Even at large attack angles where the Water Tunnel data may be in error, the results are as satisfactory as those from the other type of tests.

**The data plotted in Figures 7 and 8 are taken from Reference (4), Figure 7, and corrected by the methods outlined on Pages 17 and 18 of that reference to give the so-called "second approximation" characteristics.**

## REYNOLDS NUMBER AND TURBULENCE EFFECTS FOR TESTS AND APPLICATIONS

The range of Reynolds numbers covered by the Water Tunnel tests includes the values characteristic of many hydrofoil applications. For very large propellers R will exceed 1,000,000, but for many pump, turbine, and small propeller applications, R is less than that figure. For application outside the range of the tests the data must be extrapolated and corrected. For test Reynolds numbers up to about 3,000,000, Wind Tunnel measurements[4] have indicated that the lift curve slope increases only one or two per cent beyond its value at R = 1,000,000. The angle for zero lift and the pitching moment coefficient are also affected only slightly. However, the maximum lift coefficient increases 10% to 20% and the profile drag coefficient decreases at approximately the same rate as the turbulent skin friction drag on flat plates. By judicious application of such rules the useful range of these results can be extended appreciably.

Actually, the performance measured in the tunnel will differ from free-stream behavior because of differences in turbulence. High turbulence in the tunnel working section will cause high maximum lift coefficients and will influence the boundary layer transition on the hydrofoil and hence $c_{d_o}$. There are methods proposed for compensating for tunnel turbulence [4] [5] by assuming the results apply at higher than test Reynolds numbers, but these procedures are of questionable accuracy for all but $c_{l_{max}}$ corrections and were not applied to the Water Tunnel data.

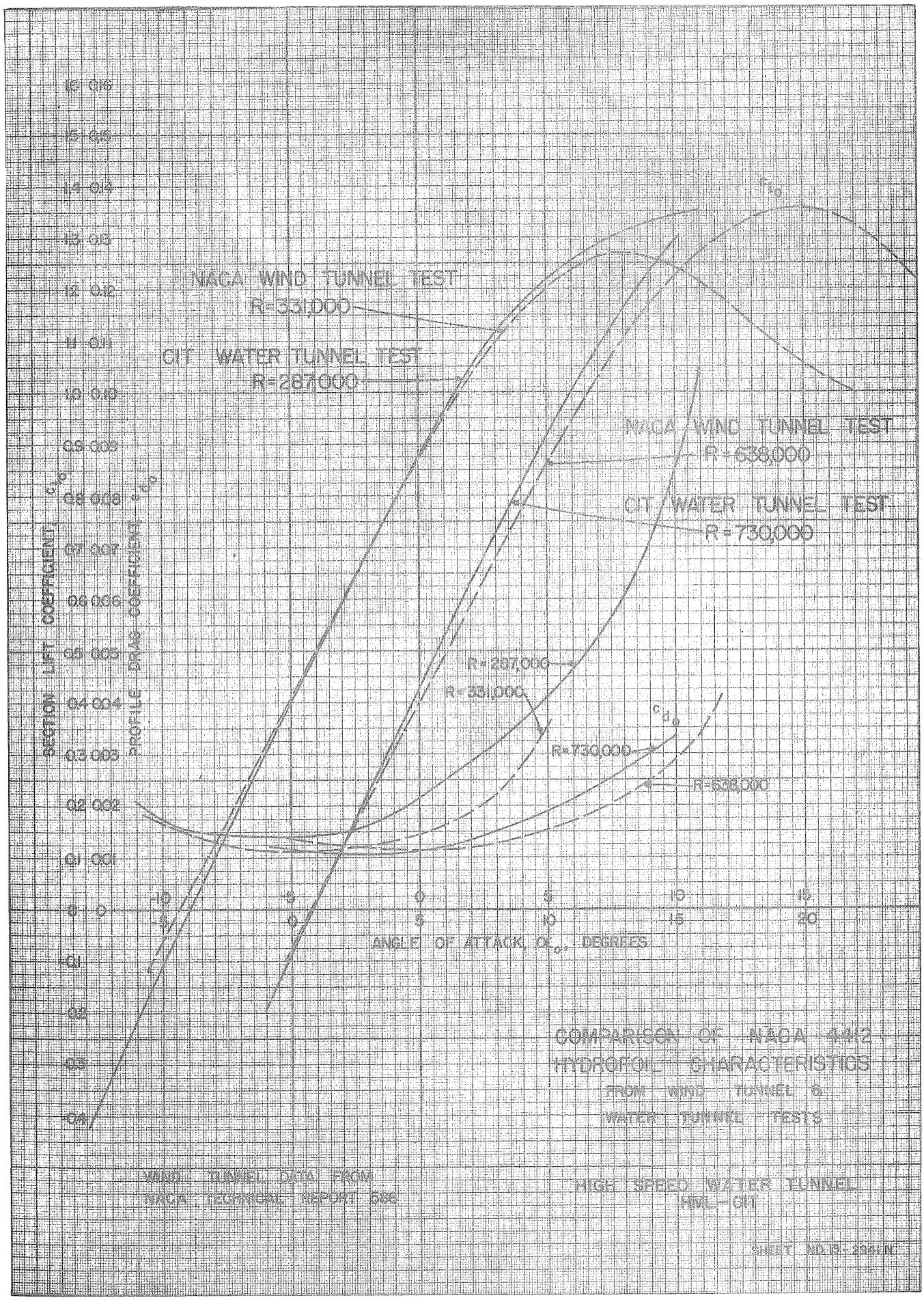
NACA WIND TUNNEL TEST
R=331,000
CIT WATER TUNNEL TEST
R=287,000
NACA WIND TUNNEL TEST
R=638,000
CIT WATER TUNNEL TEST
R=730,000
R=287,000
R=331,000
R=730,000
R=638,000
SECTION LIFT COEFFICIENT
PROFILE DRAG COEFFICIENT
ANGLE OF ATTACK, $\alpha_o$, DEGREES
COMPARISON OF NACA 4412
HYDROFOIL CHARACTERISTICS
FROM WIND TUNNEL &
WATER TUNNEL TESTS
WIND TUNNEL DATA FROM
NACA TECHNICAL REPORT 586
HIGH SPEED WATER TUNNEL
HML-CIT
SHEET NO. P-284-N

FIGURE 7

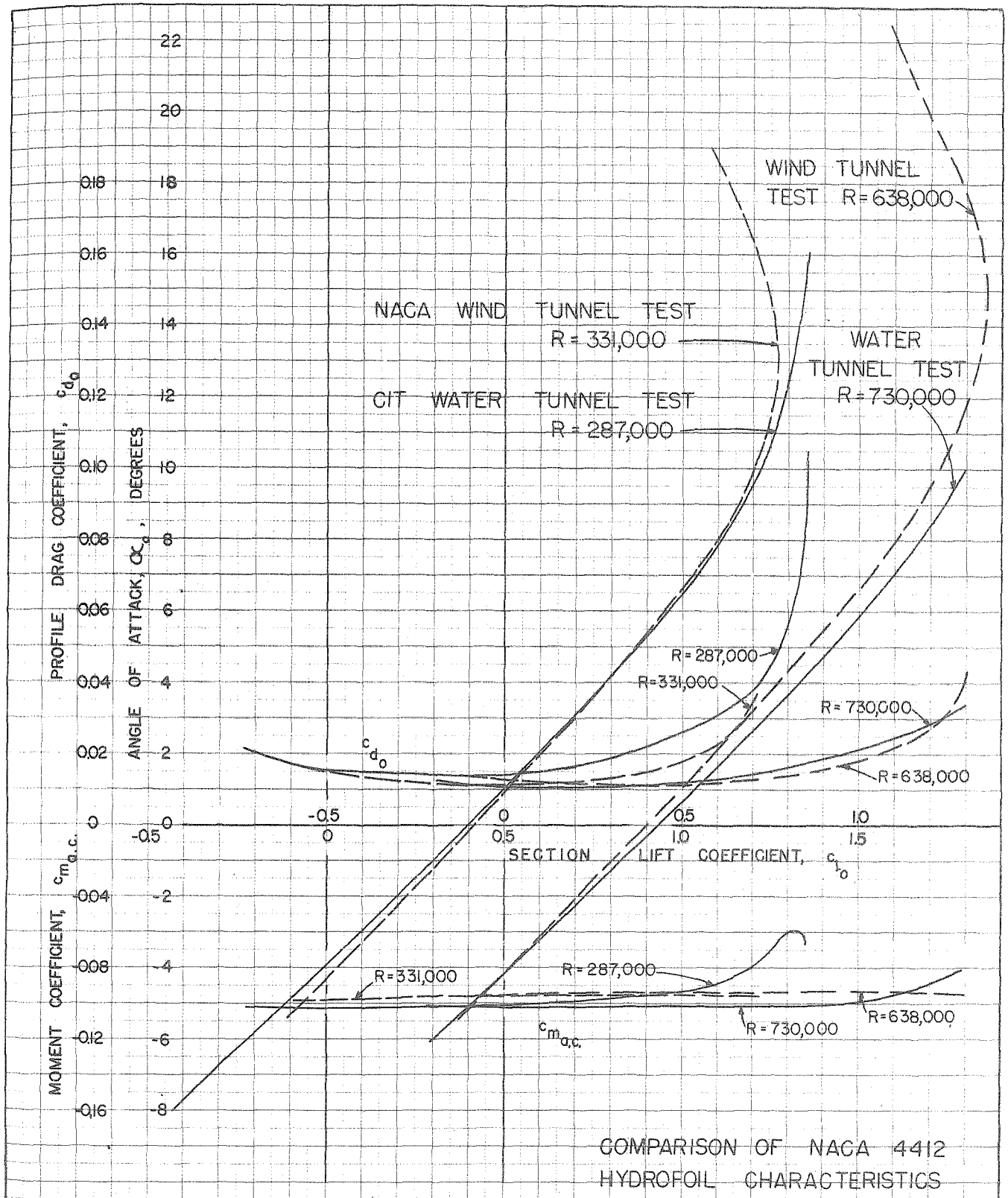


COMPARISON OF NACA 4412 HYDROFOIL CHARACTERISTICS FROM WIND TUNNEL & WATER TUNNEL TESTS

WIND TUNNEL DATA FROM NACA TECHNICAL REPORT 586

HIGH SPEED WATER TUNNEL HML – CIT

SHEET ND 19 - 2940 N

FIGURE 8

## IV. CAVITATION CHARACTERISTICS

The continuity of the behavior of airfoils when used in the normal range of velocities below the sonic is limited by "separation" of the flow for large angles of attack. For the same shape used as a hydrofoil in a liquid instead of a gas the continuity in behavior can be interrupted by cavitation as well as by separation. Cavitation occurs when, because of flow accelerations caused by the curvatures of the hydrofoil, the local pressure at any point on the hydrofoil is reduced to the vapor pressure of the liquid. This results in local boiling and vapor bubble formation. These bubbles collapse as they are swept into higher pressure zones. As the flow velocity is increased or as the general pressure level is reduced, the extent of the low pressure zone is enlarged and the volume occupied by cavitation bubbles increases.

The interest in cavitation lies in the fact first, that when it begins the lift on the hydrofoil (or thrust for propellers) drops off sharply and the drag simultaneously increases. Second, prolonged cavitation causes physical damage to the hydrofoil blade itself. Cavitation erosion of propellers and turbine impellers are two outstanding examples of this latter.

### THE CAVITATION PARAMETER, K

The influence of pressure and velocity on the inception and development of cavitation is represented conveniently by a parameter defined as

$$K = \frac{P_L - P_b}{\rho \frac{V^2}{2}}$$

where

$P_L$ = absolute pressure in the undisturbed flow in pounds per square foot

$P_b$ = absolute pressure in the cavitation bubble, taken as the vapor pressure of the fluid in these tests in pounds per square foot

$\rho$ = density of fluid in slugs per cubic foot

$V$ = velocity in feet per second

$P_L - P_b$ is a measure of the margin of pressure above that at which local boiling and hence cavitation can occur. $\rho \frac{V^2}{2}$ is a measure

of the possible local pressure reduction caused by local flow accelerations on the body. Thus either a decrease in $P_L$ or an increase in V will produce a tendency to cavitate. K will have a certain critical value at the inception of cavitation on any body so that for a given velocity and critical K, $P_L$ is the pressure at which cavitation first occurs. Or for a given pressure difference, $P_L - P_b$, V is the velocity at which cavitation begins. Each advanced stage of cavitation is described by successively lower values of K and the degree and general appearance of the cavitation can be reproduced by adjusting pressure and velocity to give the desired K.

## CAVITATION PHOTOGRAPHS

Under suitable test conditions the inception and development of cavitation can be observed and photographed. Figures 10 to 50 inclusive make up a photographic study of the cavitation on the NACA 4412 hydrofoil. These flash photographs of about 20 microseconds exposure were obtained at constant water speed and variable pressure by the test methods described in Appendix A. They include the development of cavitation on one or both faces of the hydrofoil for attack angles ranging from $-4^\circ$ to $+12^\circ$. The photographs are grouped according to angle of attack, each group arranged to show the development of cavitation as the pressure and, hence, the cavitation parameter, K, is reduced. Figure 9 is a diagram that will be useful in discussing the significance of the pictures. It is a graph of the cavitation parameter, K, plotted against the angle of attack, $\alpha_o$. A curve marks the inception of cavitation on the upper and the lower surface of the hydrofoil. In the area above this curve there is no cavitation, while everywhere below the curve cavitation exists in varying degrees, increasing with the reduction of K below the incipient value. The numbers of 10 to 50 appearing on the diagram refer to figures in the report and the coordinates of the points marked by the numbers indicate the attack angle and K value at which each picture was taken. Thus the relationship between conditions for inception of cavitation and the conditions for each figure is shown graphically.

## ANGLE OF ATTACK AND CAVITATION INCEPTION

It will be noted in Figure 9 that for both large positive and large negative angles of attack, cavitation occurs "early" that is, at high pressures or low velocities and hence high K values. At angles near zero, cavitation is delayed, the minimum critical K falling at about 0.66 at $\alpha_o = -1.14^\circ$. Thus, Figure 38 shows cavitation soon after inception at K = 1.8 for $\alpha_o = +8^\circ$, while Figure 19 shows the beginning of cavitation at K = 0.57 for $\alpha_o = 0^\circ$. This is caused by the fact that with increasing attack angle the leading edge of the hydrofoil, where the profile curvature is large, is turned at an angle to the flow and the water must curve

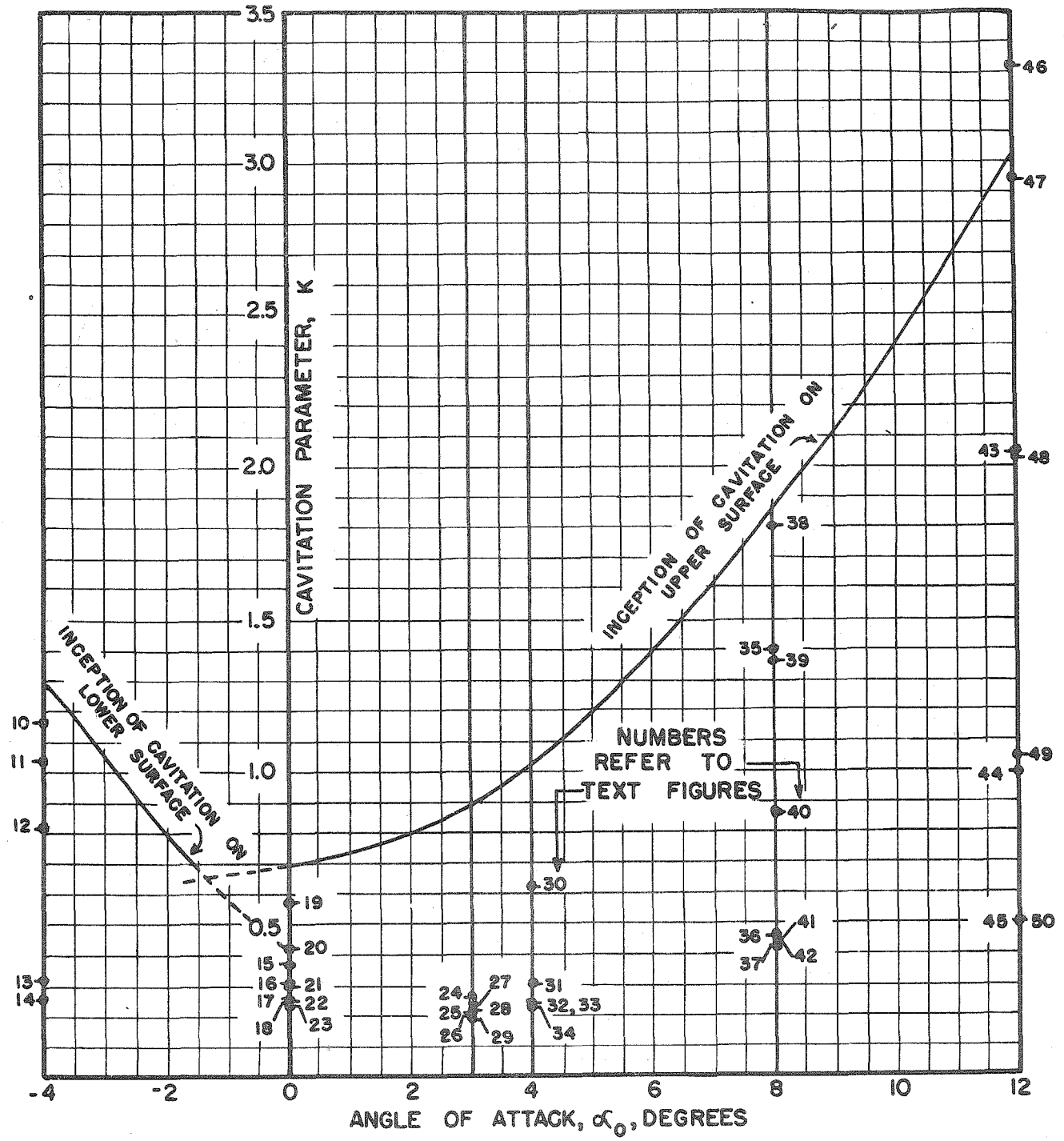


## NACA 4412 HYDROFOIL CAVITATION

DIAGRAM SHOWING TEST CONDITIONS
FOR EACH PHOTOGRAPH
IN FIGURES 10 TO 50

CIT — HML
ND 19 — 2977 — L



FIGURE 9

NACA 4412 HYDROFOIL
LOWER SURFACE $\alpha = -4^{0}$
V = 45 FT/SEC

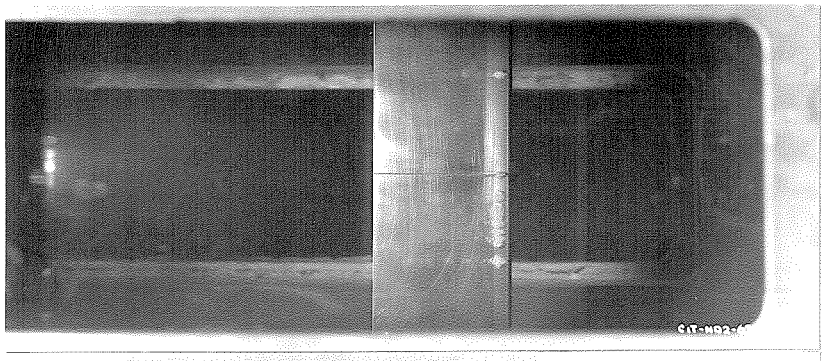

FIGURE 10
K = 1.17

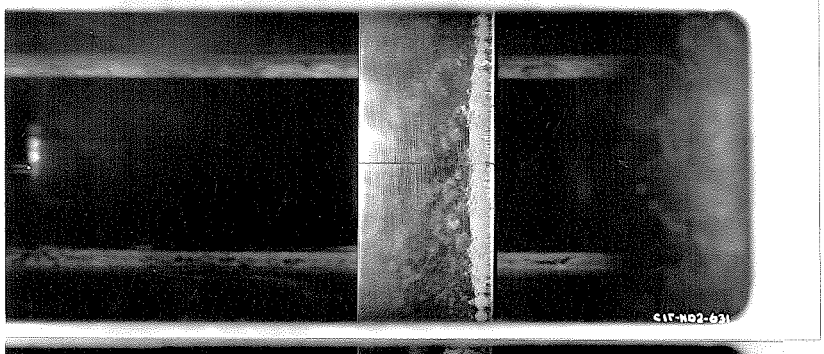

FIGURE 11
K = 1.04

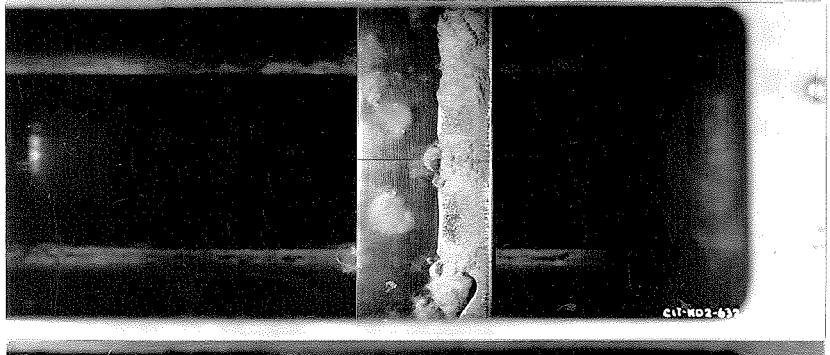

FIGURE 12
K = 0.82

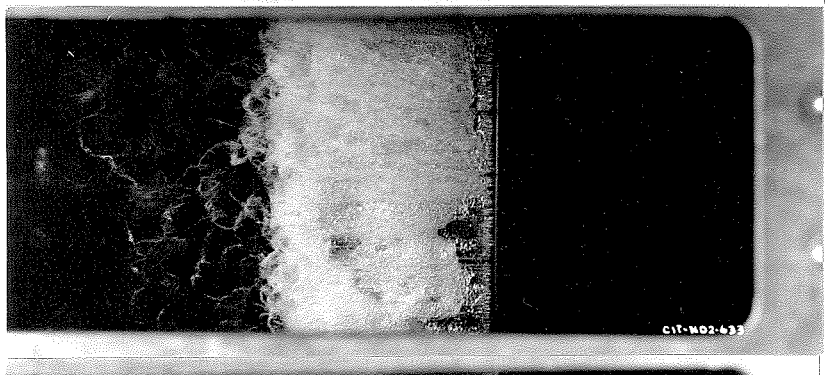

FIGURE 13
K = 0.32

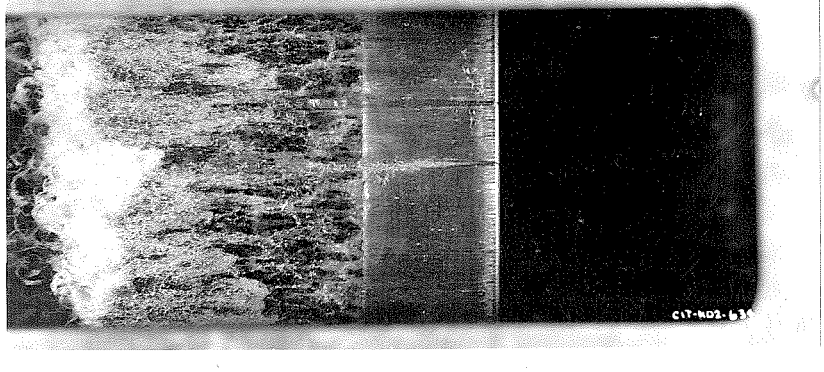

FIGURE 14
K = 0.26

FIGURE 15
$K = 0.37$

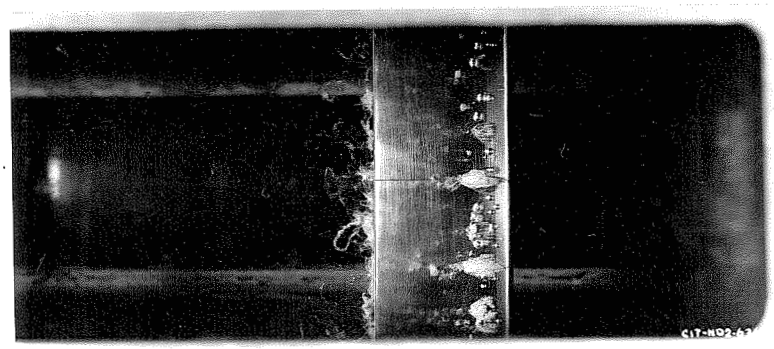

FIGURE 16
$K = 0.31$

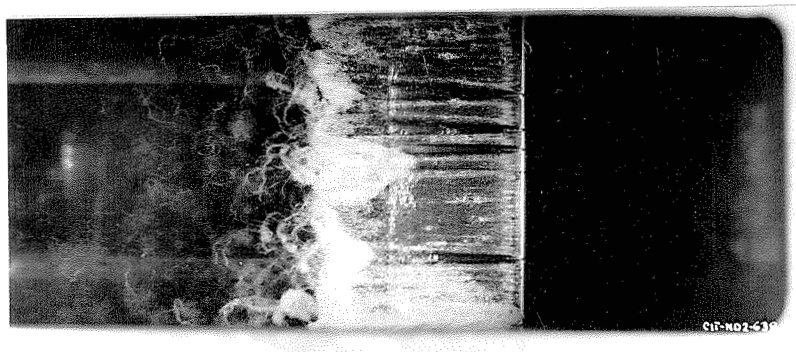

FIGURE 17
$K = 0.26$
(BACK LIGHTING)

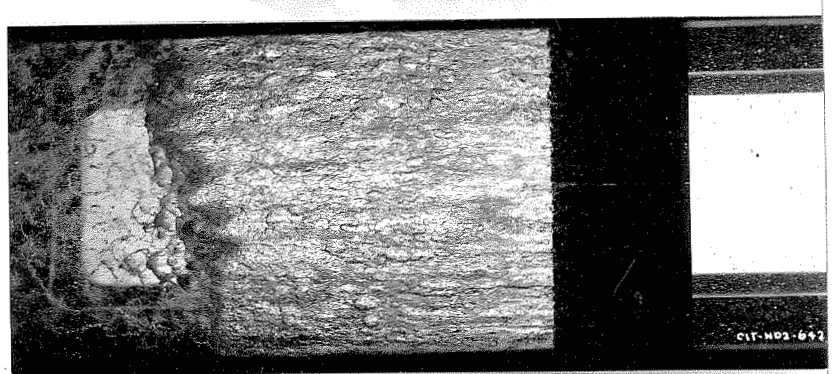

FIGURE 18
$K = 0.24$

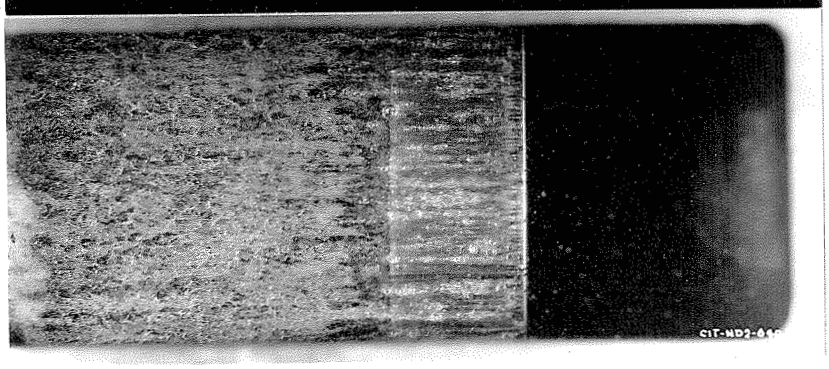

NACA 4412 HYDROFOIL
UPPER SURFACE $\alpha = 0^{\circ}$
V = 45 FT/SEC

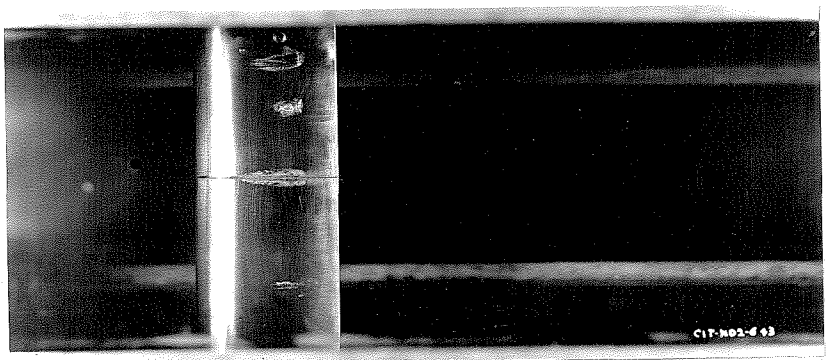

FIGURE 19
K = 0.57

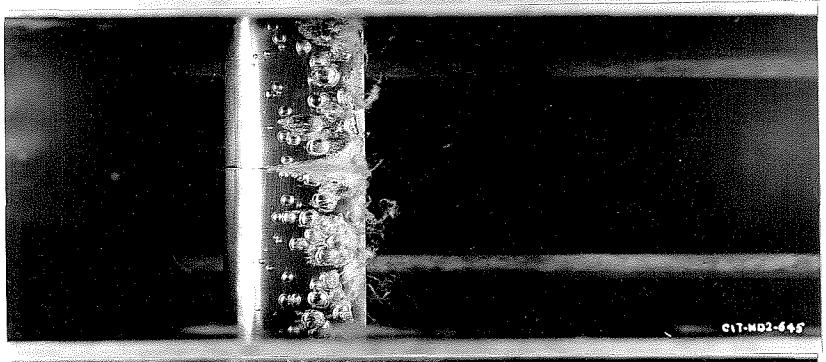

FIGURE 20
K = 0.42

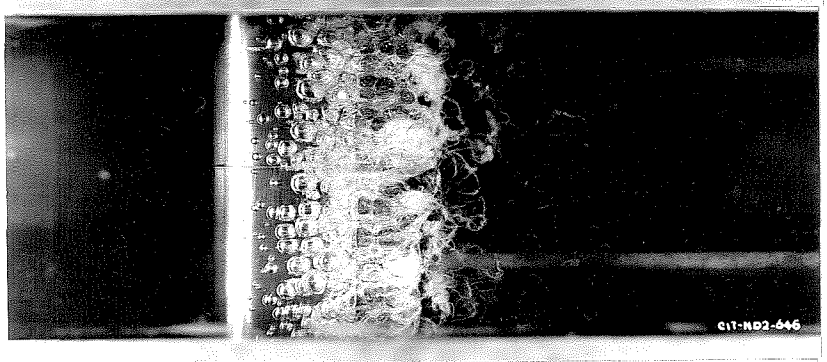

FIGURE 21
K = 0.30

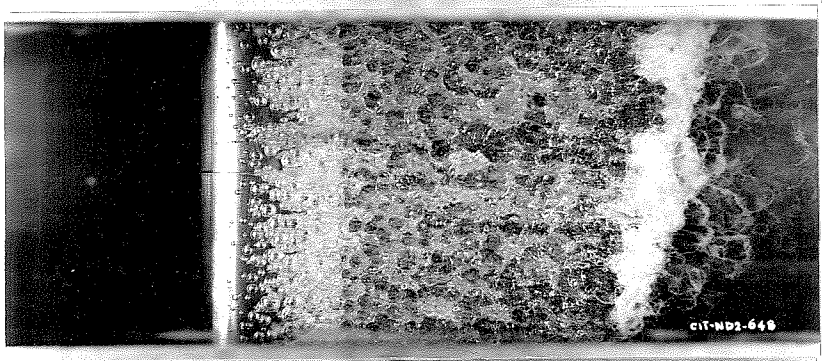

FIGURE 22
K = 0.25

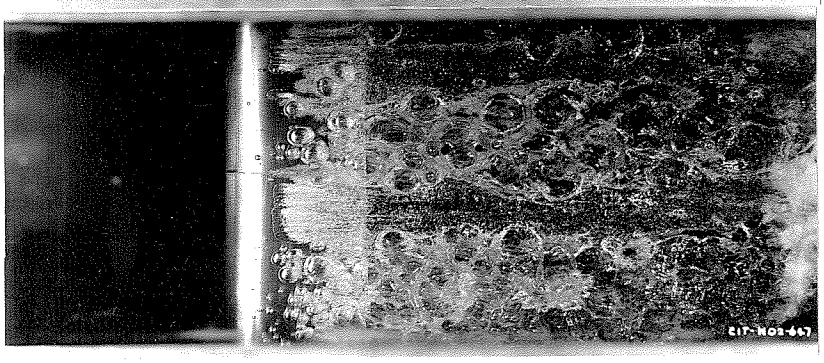

FIGURE 23
K = 0.24

NACA 4412 HYDROFOIL
LOWER SURFACE $\alpha = +3^{0}$ (APPROX)
V = 40 FT/SEC



FIGURE 24
K = 0.26


FIGURE 25
K = 0.21

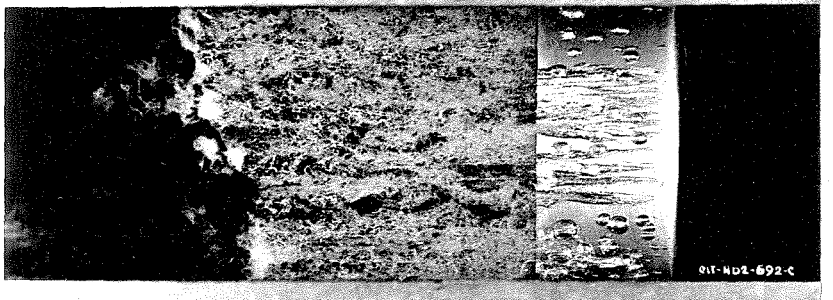


FIGURE 26
K = 0.20

NACA 4412 HYDROFOIL
UPPER SURFACE $\alpha = +3^{\circ}$ (APPROX)
V = 40 FT/SEC


FIGURE 27
K = 0.24

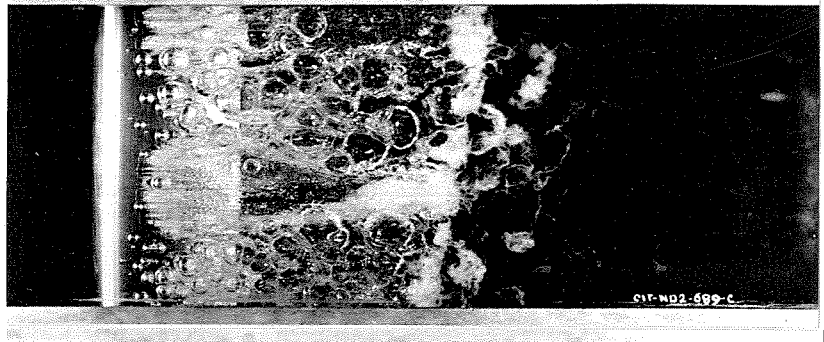


FIGURE 28
K = 0.22

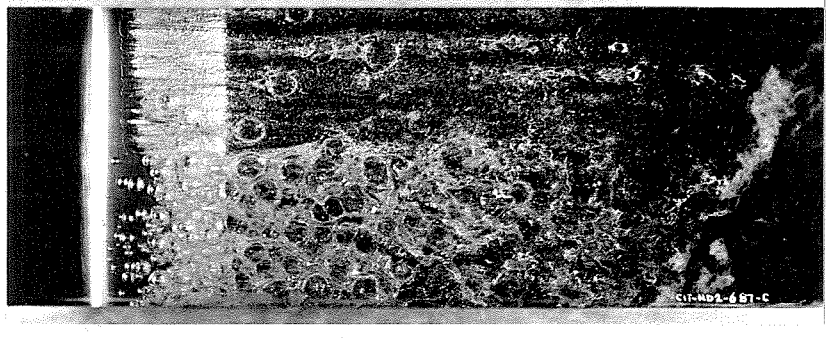


FIGURE 29
K = 0.19

NACA 4412 HYDROFOIL
UPPER SURFACE $\alpha = +4^{0}$
V = 45 FT/SEC

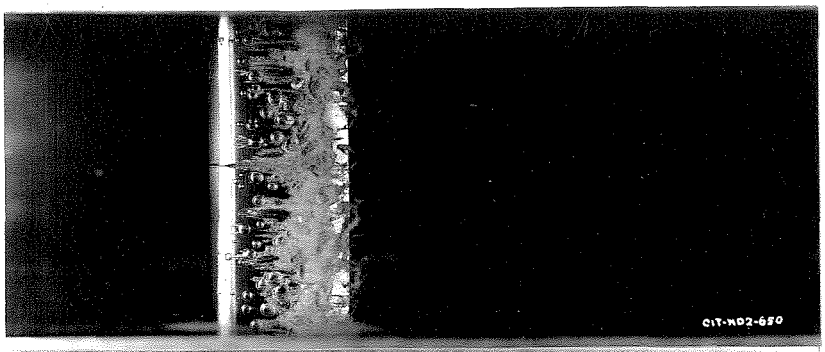


FIGURE 30
K = 0.62

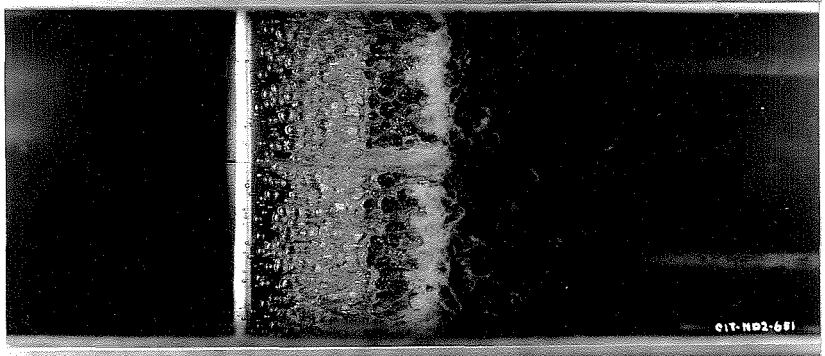


FIGURE 31
K = 0.30

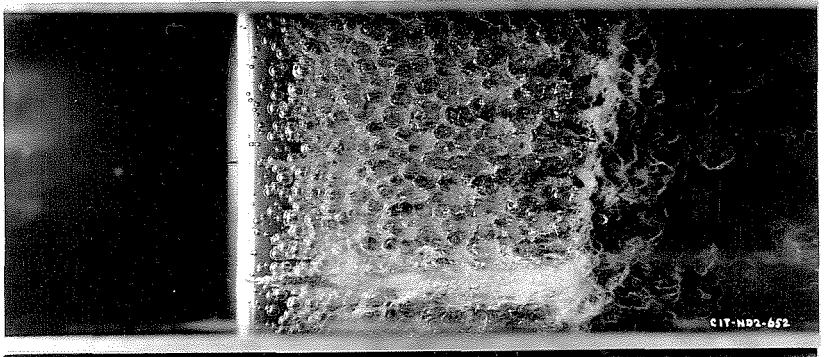


FIGURE 32
K = 0.24

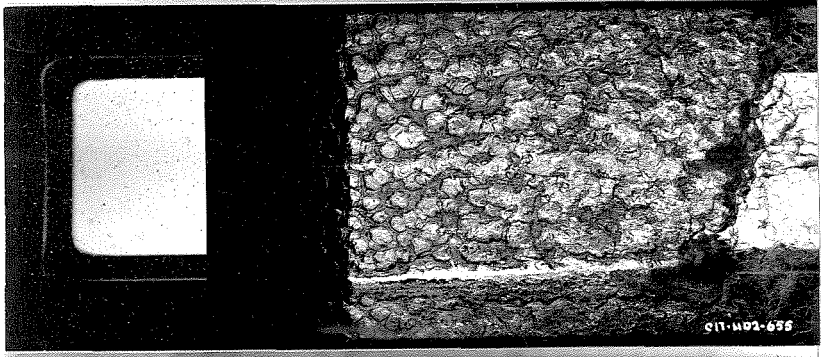


FIGURE 33
K = 0.24
(BACK LIGHTING)

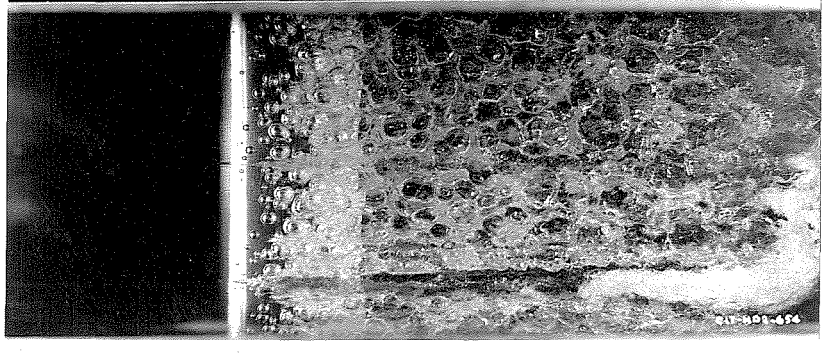


FIGURE 34
K = 0.23
(ESTIMATE)

FIGURE 35
K = 1.39

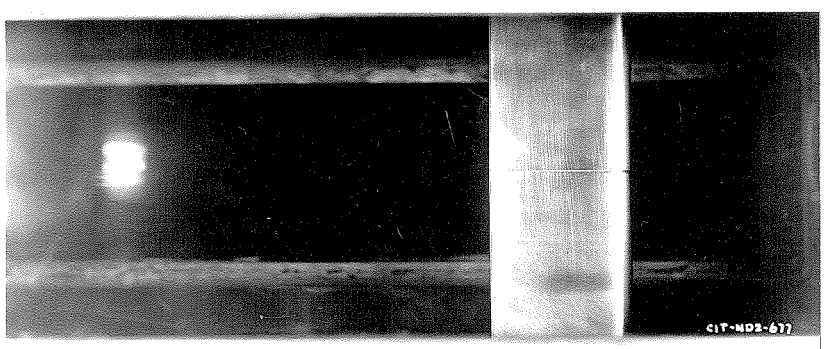


FIGURE 36
K = 0.26


FIGURE 37
K = 0.23

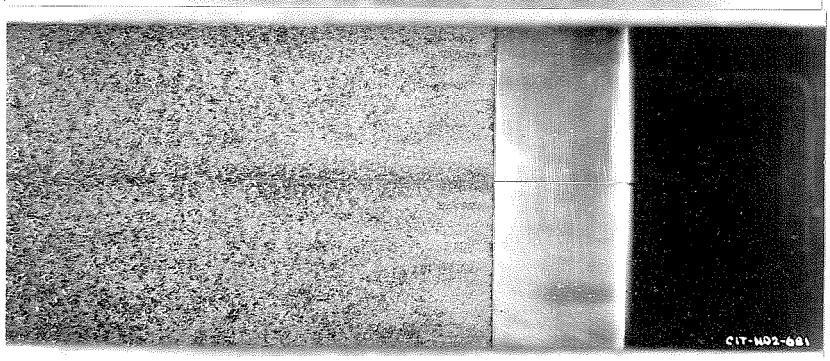

NACA 4412 HYDROFOIL
UPPER SURFACE $\alpha = +8^{0}$
V = 45 FT/SEC

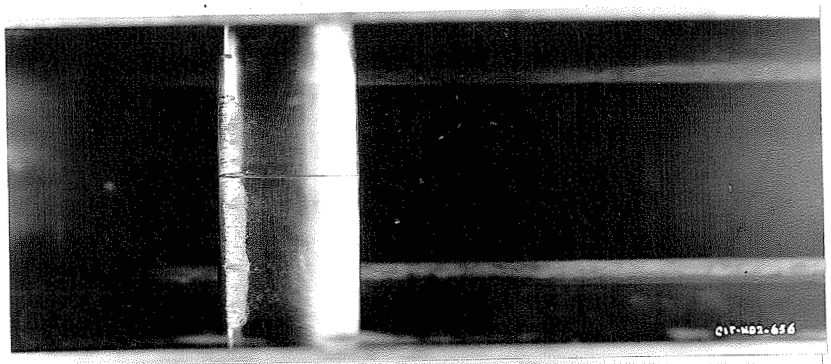


FIGURE 38
K = 1.8


FIGURE 39
K = 1.36

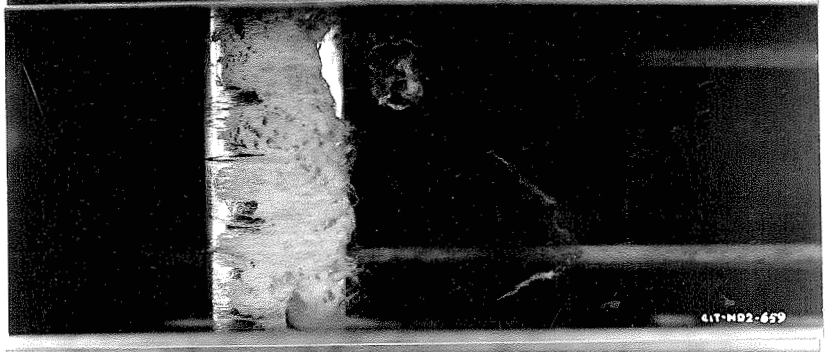


FIGURE 40
K = 0.86

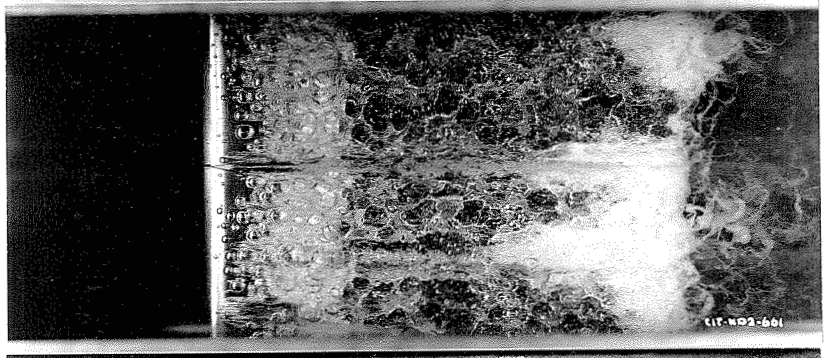


FIGURE 41
K = 0.25

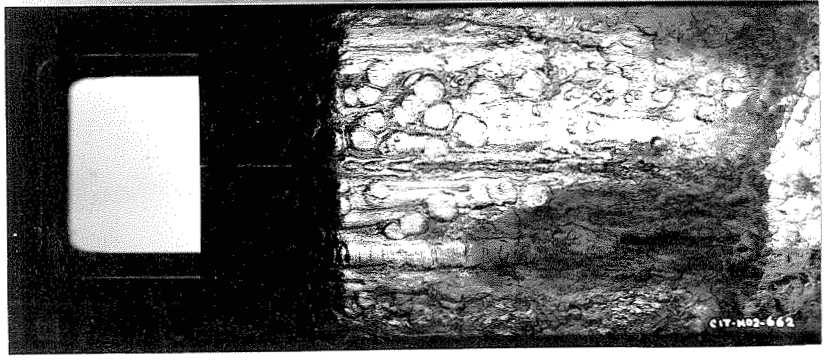


FIGURE 42
K = 0.24
(BACK LIGHTING)

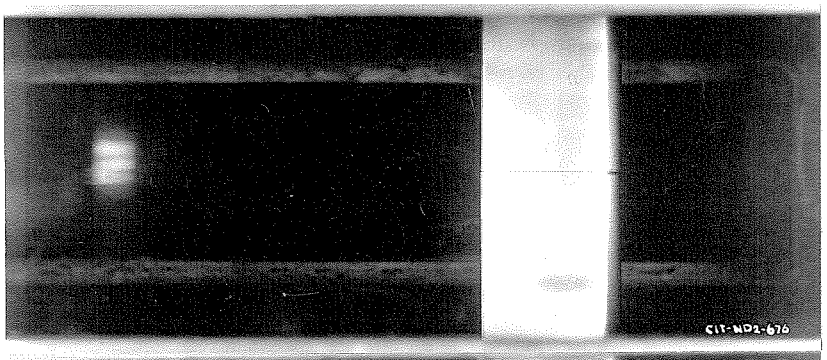


FIGURE 43
K = 2.04

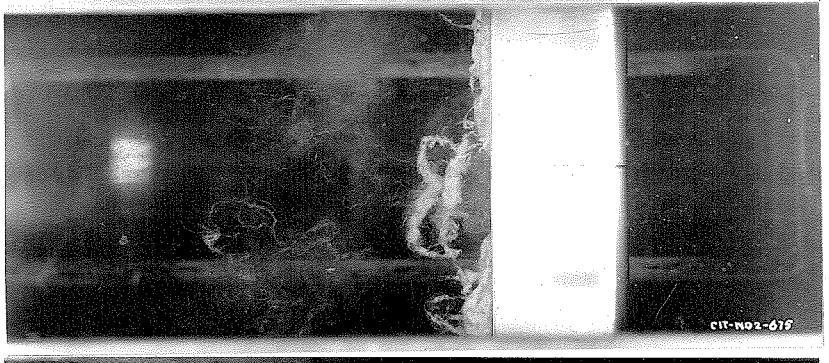


FIGURE 44
K = 0.99

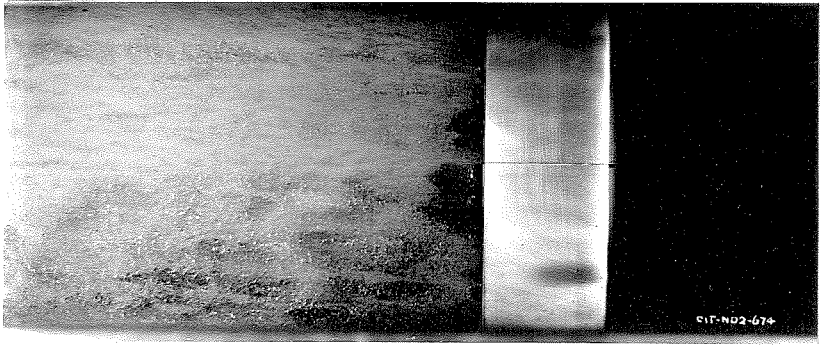


FIGURE 45
K = 0.30

NACA 4412 HYDROFOIL
UPPER SURFACE $\alpha = +12^{\circ}$
V = 35 FT/SEC

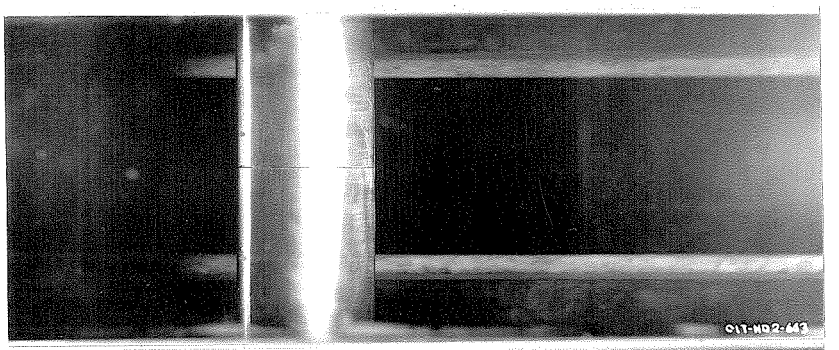

FIGURE 46
K = 3.31

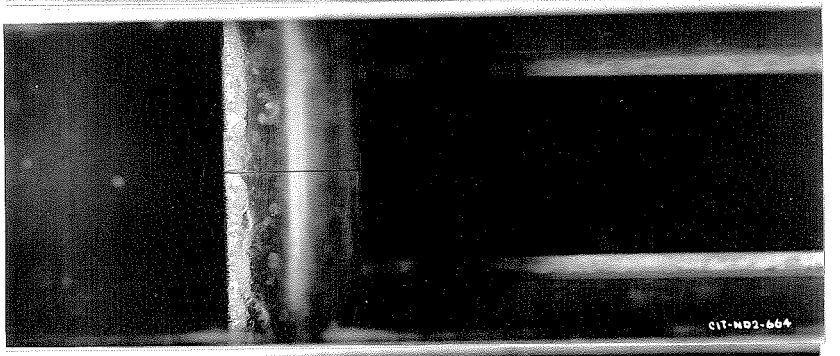


FIGURE 47
K = 2.94

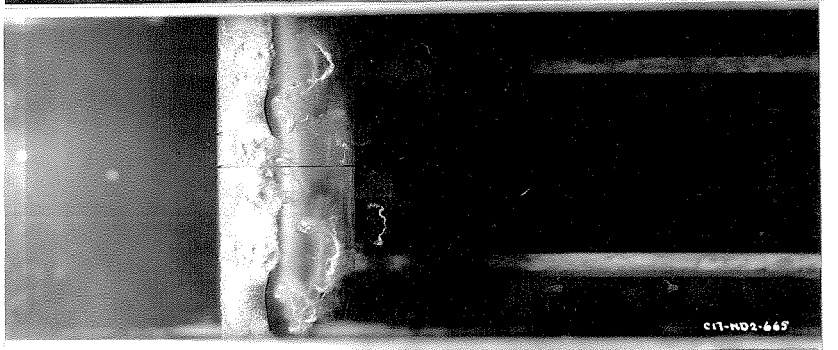


FIGURE 48
K = 2.02

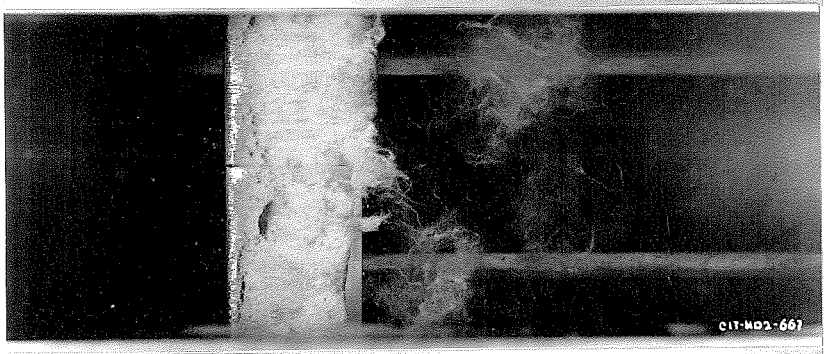


FIGURE 49
K = 1.05

FIGURE 50
K = 0.30

sharply to follow it. Consequently, the local acceleration of the fluid is large and the vapor pressure is reached locally even with high static pressure in the main flow. In both Figures 38 and 19 cavitation is occurring first on the top surface of the hydrofoil because it is the low pressure side for those attack angles. At negative angles beyond $-1.4^{\circ}$, however, the higher pressure is obtained at the top and cavitation occurs first on the lower surface. Thus in Figure 10, for $\alpha = -4^{\circ}$, the beginning of cavitation is shown near the leading edge of the lower side if the hydrofoil.

At high angles of attack cavitation occurs only on one surface of the hydrofoil. There is a sufficient dynamic pressure increase on the surface pitched into the stream to suppress cavitation completely. Figures 43 to 50 show that for $\alpha_0 = 12^{\circ}$ no cavitation is obtained on the lower surface of the hydrofoil even though K is reduced to 0.3, while on the upper surface cavitation is well established at K = 2.94. For angles near zero, cavitation occurs first on the upper or low pressure surface and then also occurs on the high pressure surface as K is reduced. For example, at $\alpha = +3^{\circ}$, the lowest pressure occurs on the top of the hydrofoil and Figure 27 shows well developed cavitation there with K = 0.24. By contrast, Figure 24 shows the bottom surface at K = 0.26 with cavitation in an early stage. This is also illustrated by Figure 15, a photograph of the lower surface at $\alpha = 0^{\circ}$ and K = 0.37. There the beginning of cavitation on the lower side is seen with trailing wisps of the more fully developed cavitation on the top appearing at the left.

CAVITATION BUBBLE GROWTH

A certain similarity exists for each sequence of photographs for one angle of attack. Cavitation begins on the forward part of the hydrofoil as a narrow zone of small bubbles. The bubbles are individually distinguishable in some cases but coalesce to form "sudsy" zones in others. The limits of the zone of bubbles is a rough measure of the extent of the low pressure area on the hydrofoil surface. As the pressure is reduced the low pressure area is broadened and the vapor bubbles are swept farther back before collapsing, until they form a sheet hiding the hydrofoil and extending downstream more than 6 or 8 chord lengths completely past the limits of the working section windows. (See Figures 23, 29, 34, etc.) For any given pressure and velocity the cavitation bubble grows until the rate of vapor entrainment by the water balances the rate of vapor formation within the bubble. Thus the magnitude of the cavitation zone in each of the photographs represents a "steady state" condition for the given value of K.

As Figures 10 to 17 show, the fine grain "sudsy" type of bubbles are obtained where the minimum pressure is caused by a sharp curvature such as occurs at the leading edge of the lower hydrofoil surface. Figures 19 to 23, on the other hand, show the formation of transparent, relatively large individual bubbles on the upper surface. Here the minimum pressure is obtained where

the profile has a more gentle curvature. As the hydrofoil is given larger angles of attack (Figures 46 to 50 at $\alpha = +12^{\circ}$, the minimum pressure point moves forward to a place where the curvature of the upper surface is sharper and the "sudsy" bubbles are again obtained.

Under some conditions the forward portion of the large enveloping bubble for fully developed cavitation is transparent. That is, the interface between the cavitating zone and the surrounding water is a smooth surface free of disturbances. An example of this is shown in Figure 14 where the hydrofoil itself and the disturbance from cavitation on the opposite face of the hydrofoil are clearly visible through the bubble enveloping the near surface. The smooth interface is an indication that very little vaporization is occurring through that surface. Most of the vapor that is being supplied to the bubble comes from the turbulent boiling zone near the downstream end of the envelope. Figure 23 shows how the bubbles tend to coalesce as the prrssure is reduced to form the single large transparent envelope. The transparency cannot always be reproduced, but rather seems to occur randomly unless some external disturbance, such as a piece of trash hanging to the foil or a nick in its surface, is introduced to accelerate the formation. Figure 16 shows the effect of small disturbances at the leading edge in forming long, extended bubbles. Such disturbances also cause cavitation to occur at higher pressures (or lower velocities) than would the hydrofoil alone. Figure 26 shows two such bubbles that are caused by small pieces of tobacco clinging to the leading edge.

Note that the individual bubbles grow from the time of their formation until they collapse. In Figure 22 measurements of the average bubble size showed that its growth was rapid for the first quarter chord length of travel, attaining 60 to 75 per cent of what appears to be the final diameter. Beyond this the bubbles grow more slowly until they interfere with their neighbors and finally are entrained and collapse. The interior of the cavitation bubble is at the vapor pressure of the water and is maintained at this pressure by the "pumping" action of the water. The growth of the bubbles is probably evidence of continual vaporization into each bubble cavity until the bubble itself is swept into a higher pressure zone.

## CRITICAL K COMPARED WITH PREDICTIONS FROM WIND TUNNEL PRESSURE DISTRIBUTION DATA

Figure 51 is another diagram showing values of the cavitation parameter, K, for incipient cavitation, vs the angle of attack, $\alpha_o$. This diagram covers a much wider range of angles than Figure 9 and includes, in addition, a curve predicted from Wind Tunnel measurements of the pressure distributions on the 4412 profile.[3] The predicted curve is obtained by subtracting the minimum pressure on

the airfoil surface from the pressure in the undisturbed flow and dividing by the dynamic head, thus

$$\frac{P_L - P_{min}}{\rho \frac{V^2}{2}}$$

where

$P_L$ = pressure in the undisturbed flow in pounds per square foot

$P_{min}$ = lowest pressure on the hydrofoil surface in pounds per square foot

$\rho$ = density of the fluid in slugs per cubic foot

$V$ = velocity in feet per second

This is identical in form with the cavitation parameter, K, so that for any velocity if $P_{min}$ is taken as the vapor pressure of water, and $P_L$ as the pressure in the undisturbed flow when cavitation first appears, the ratio has the same value as critical K.

The agreement between the Water Tunnel curve and the predicted curve is good for angles of attack within the normal useful range, but the two curves diverge when $\alpha_o$ becomes very large, either negatively or positively. The reason for this difference is unknown but several factors could contribute to it. At large angles of attack very small differences in profile curvature at the leading edge will materially affect the minimum pressure obtained. Also it is in this range that greatest deviations from true infinite aspect ratio free stream conditions exist for both the finite span used in the Wind Tunnel test and the two-dimensional installation used in these tests.

CRITICAL K VS SECTION LIFT COEFFICIENT

For some purposes it is more convenient to refer the critical value of K to the lift coefficient instead of the angle of attack. Thus on Figure 52, K is plotted as a function of $c_{l_o}$. Note that this is the lift coefficient obtained *before* cavitation sets in. At any lift coefficient cavitation-free operation is possible as long as K is greater than the value shown by the curve. A qualitative investigation in the Water Tunnel showed that soon after the inception of cavitation the lift drops off sharply so that the diagram no longer applies.

## SUBMERGENCE REQUIRED TO PREVENT CAVITATION

Figure 53 shows the submergence required to prevent cavitation on the 4412 hydrofoil as a function of velocity and angle of attack. The term "submergence" means the vertical depth below the water surface (e.g., ocean surface). In each of the two diagrams the vertical distance down from the horizontal axis represents the submergence required to prevent cavitation at a given attack angle or given velocity. All points below the constant $\alpha_o$ or constant V curves represent cavitation-free operation.

The left-hand figure shows that for a velocity of 70 feet per second (41.5 knots) the minimum submergence required to prevent cavitation is 19 feet at $\alpha_o = -1.4^o$. For any other angle of attack the necessary submergence is greater. For example, at $\alpha_o = +4^o$ ($c_{l_o} = 0.8$ from Figure 4), the minimum submergence is 44 feet at 70 feet per second. In the right-hand diagram the limiting range of angles at given velocities and submergences are emphasized. For example, at 60 feet per second and 15 feet submergence, cavitation-free operation is possible only within the limits of $-2.4^o$ and $+2.6^o$.

## CAVITATION AND NOISE

With the inception of cavitation, both audible and supersonic noise is emitted from the cavitating zone. Measurements of noise caused by cavitation on various shaped bodies [10] have shown that in the high frequency range the "sound" increases by as much as 40 decibels as cavitation just begins. The source of the noise is apparently in the collapse of the vapor bubbles and the highest intensity is obtained when these bubbles are small and originate and collapse on the surface of the object. With continued growth of cavitation the vapor bubbles collapse in the water away from the body and the noise intensity is reduced considerably.

It is interesting to note that injecting a gas into the cavitating zone will cause an immediate noise reduction. This occurs because the air effectively dampens the bubble collapse.

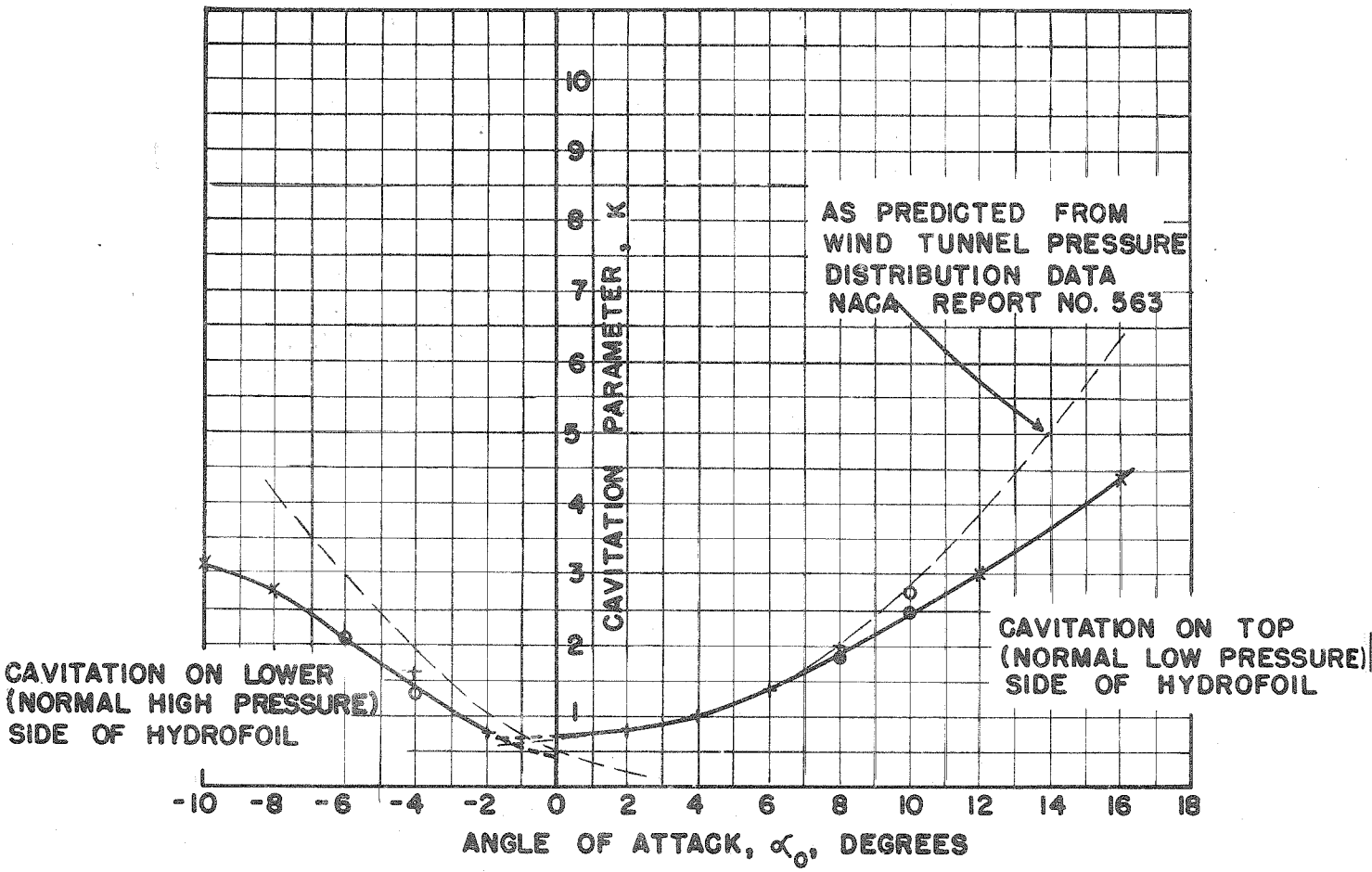


VALUES OF "K" AT WHICH CAVITATION BEGINS ON THE NACA 4412 HYDROFOIL VS. ANGLE OF ATTACK

CIT — HML
SHEET ND 19-2871 L

FIGURE 51

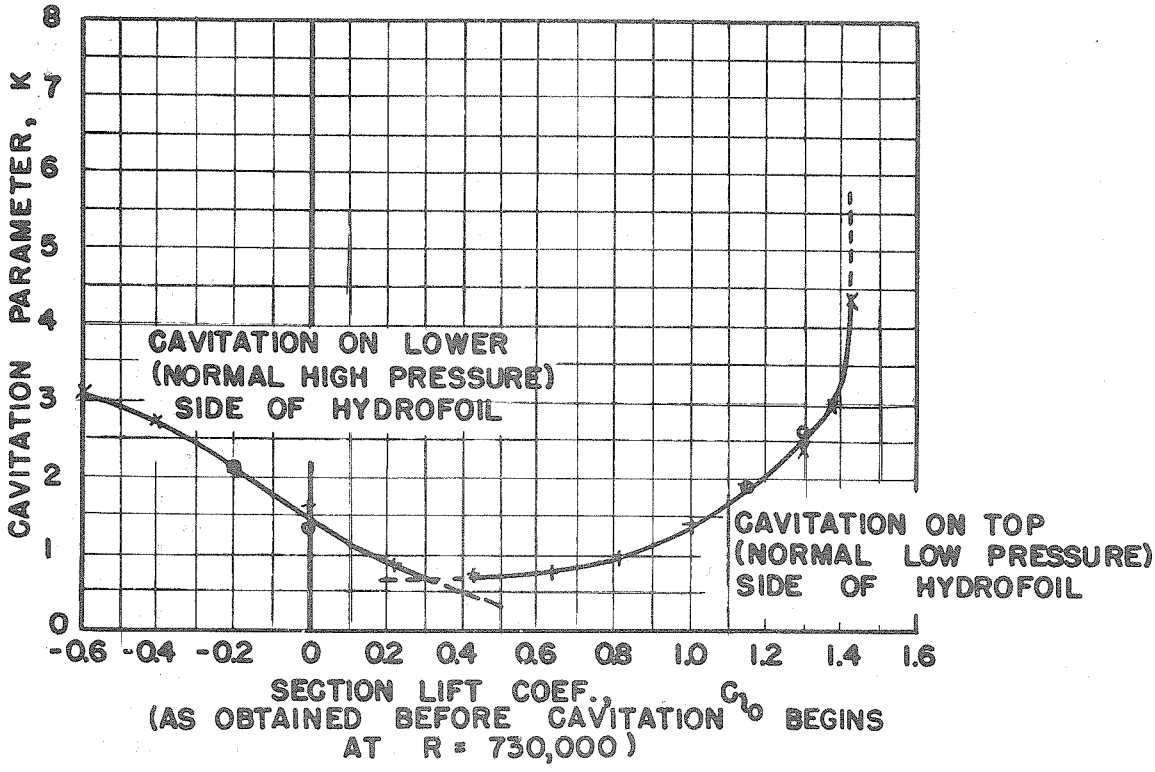


VALUES OF "K" AT WHICH CAVITATION BEGINS ON THE NACA 4412 HYDROFOIL VS. SECTION LIFT COEF.

CIT - HML
SHEET ND 19 - 2872 L

FIGURE 52

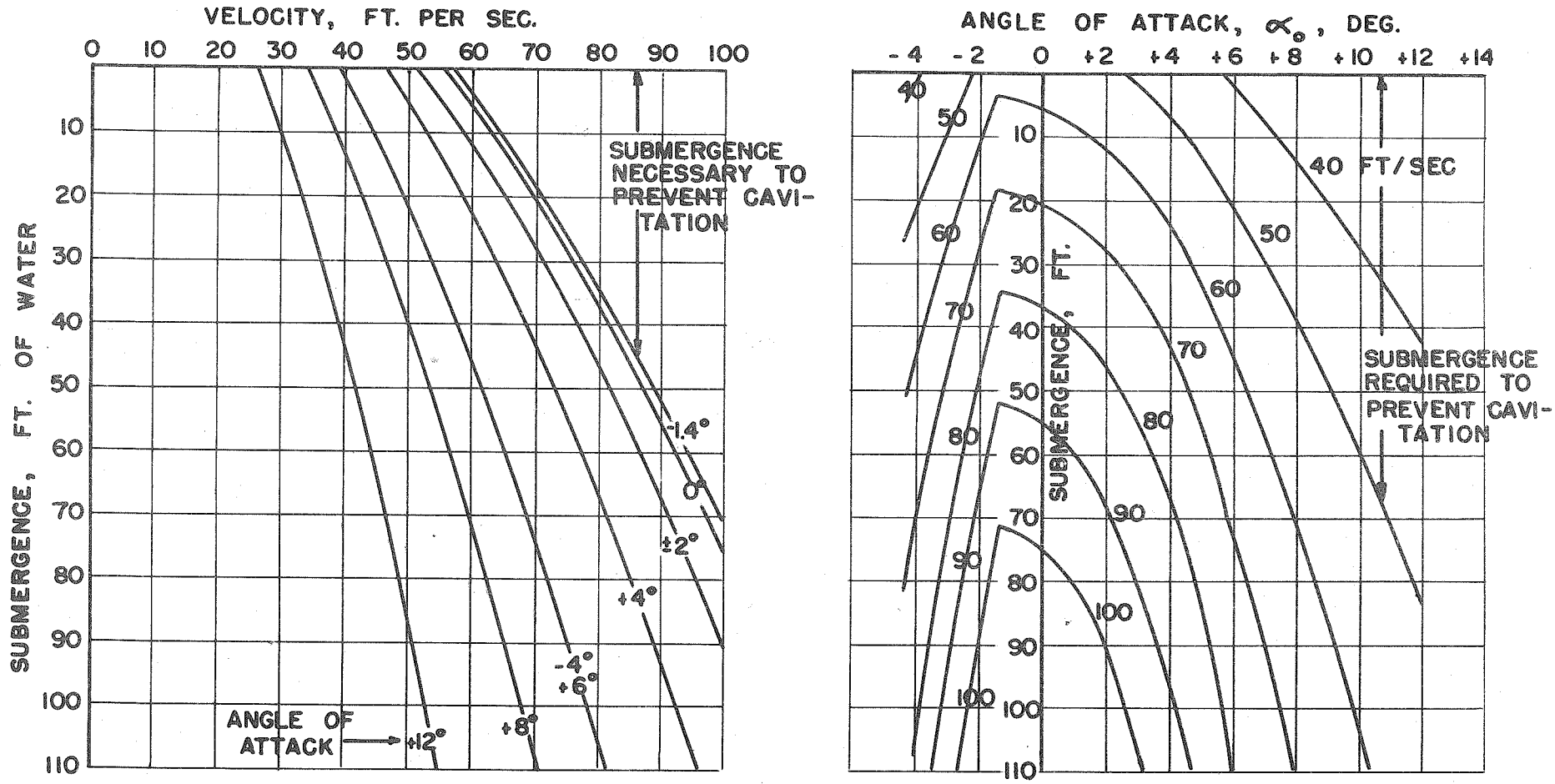


FIGURE 53

## SUBMERGENCE REQUIRED TO PREVENT CAVITATION ON NACA 4412 HYDROFOIL

CIT — HML

SHEET ND 19 - 2873 L



RESTRICTED

## V. CONCLUSIONS ABOUT METHODS OF TESTING HYDROFOILS

This report presents the results of Water Tunnel tests for the complete hydrodynamic characteristics of the 4412 profile and compares them with the available information from Wind Tunnel tests of the same shape. Aside from the specific detailed behavior of this hydrofoil the following conclusions seem evident.

Water Tunnel tests using two-dimensional hydrofoil spans provide a method of obtaining satisfactory infinite aspect ratio characteristics without making corrections of any kind to the measured data. At small angles of attack, that is at low lifts, good accuracy can be expected. Errors are to be expected at large attack angles, that is at high lifts, but this is outside the normal range of applications for hydrofoils. Even for this region the method of testing should provide satisfactory comparative data for different sections. In addition, comparison with the Wind Tunnel tests shows the Water Tunnel measurements over the entire range of angles to be as good or better than finite aspect ratio tests requiring elaborate corrections to obtain infinite aspect ratio characteristics.

Cavitation tests provide information about the inception and growth of the cavitation bubbles, about the hydrodynamic forces acting on the hydrofoil when cavitation begins, and about the consequent limitations on operating speeds and submergences. The inception of cavitation can be predicted approximately from pressure distribution measurements, but the latter are troublesome to make and are not as satisfactory as actual cavitation tests. The other information can be obtained only with underwater cavitation tests.

It seems apparent that the Water Tunnel equipped for measuring hydrodynamic forces and moments, as well as for obtaining cavitation, provides a most satisfactory means of investigating hydrofoil characteristics.

# APPENDIX A

## TEST EQUIPMENT AND PROCEDURES

The tests covered by this report were conducted in the High Speed Water Tunnel at the California Institute of Technology. The following paragraphs contain a brief description of the tunnel and the test procedures employed. A more detailed description of the High Speed Water Tunnel will be found in Reference 1.

### MAIN CIRCUIT

The Water Tunnel is of the closed circuit, closed working section type. Figure A-1 shows a profile of the main flow circuit which consists essentially of the working section, the circulating pump, the stilling tank, and the necessary pipe connections. The cylindrical working section is 14" in diameter, 72" long, and is provided with three lucite windows. The propeller-type circulating pump is V-belt connected to a variable speed dynamometer. The speed of the dynamometer is automatically controlled and is held constant within ± 1 r.p.m., which corresponds to a maximum water velocity variation in the working section of 1/30 ft. per sec. While most tests are made with water velocities of 24 to 31 ft. per sec., any velocity between 10 and 72 ft. per sec. is easily obtainable.

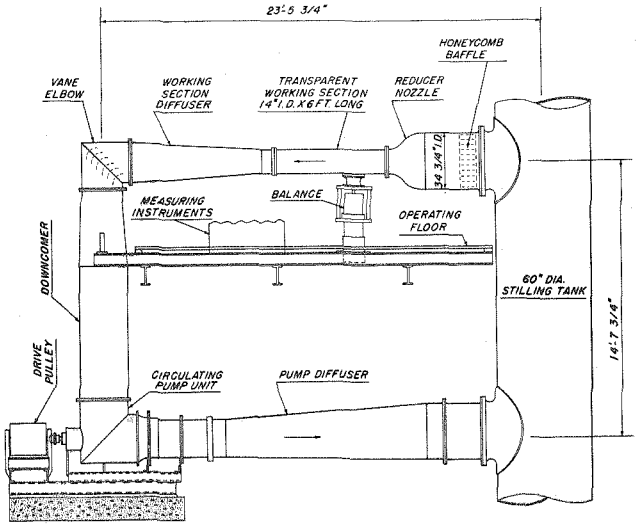


FIGURE A-1

### AUXILIARY CIRCUITS

Two auxiliary water circuits, one for pressure control and one for temperature control, are used in conjunction with the main circuit. These circuits are shown in Figure A-2, which is an isometric diagram of the complete water tunnel installation.

To make it possible to induce or inhibit cavitation at will, it is necessary that the pressure in the working section be controllable independently of the velocity. This is accomplished by superimposing the pressure regulating circuit on the main circuit.

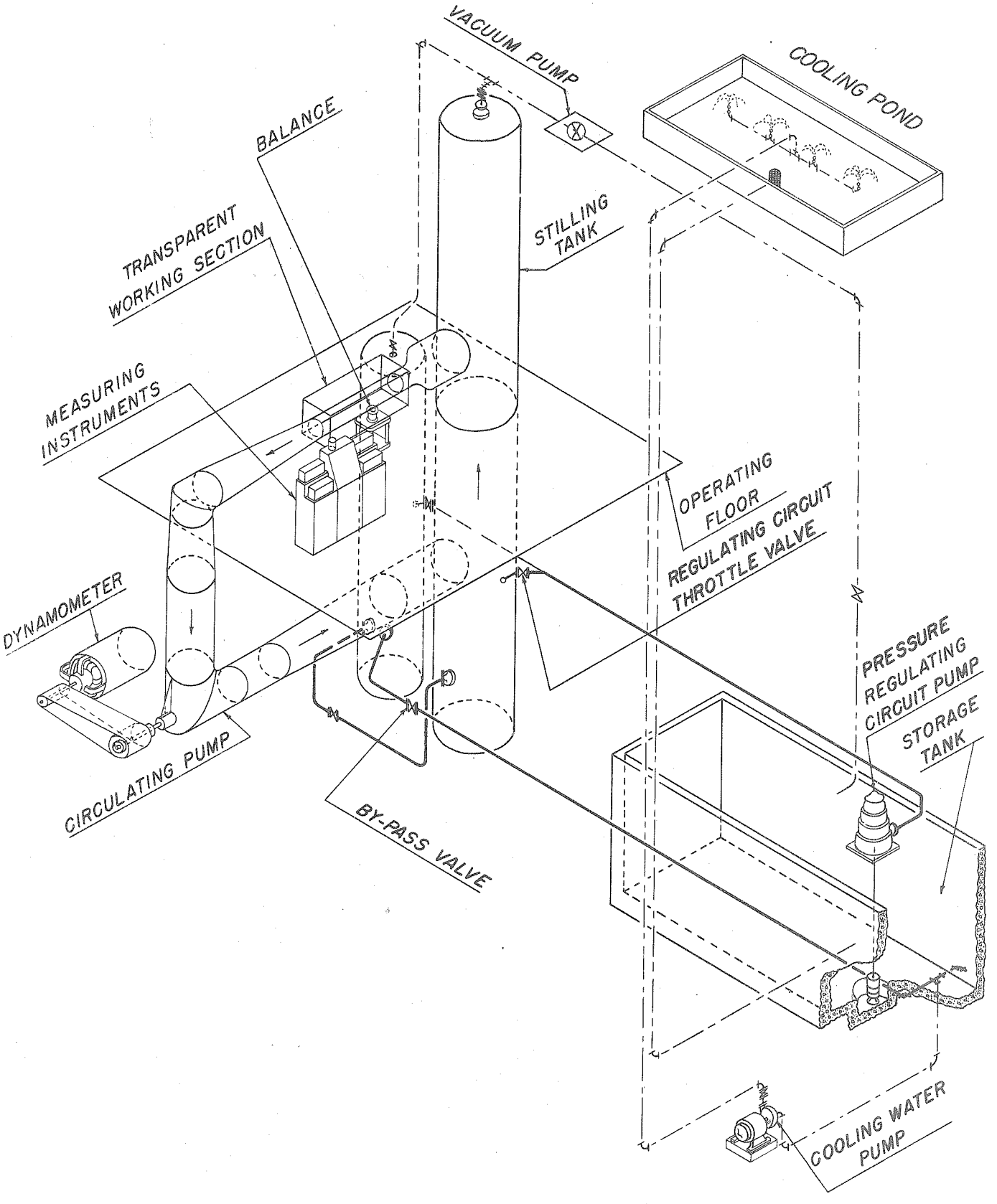
VACUUM PUMP
COOLING POND
BALANCE
TRANSPARENT WORKING SECTION
STILLING TANK
MEASURING INSTRUMENTS
OPERATING FLOOR
REGULATING CIRCUIT THROTTLE VALVE
DYNAMOMETER
PRESSURE REGULATING CIRCUIT PUMP
STORAGE TANK
CIRCULATING PUMP
BY-PASS VALVE
COOLING WATER PUMP

FIGURE A-2

A small flow of water from the sump is forced into the stilling tank by the regulating pump, and is returned to the sump through the by-pass valve. Since the main circuit is closed and completely filled, it is evident that the pressure in it may be controlled by varying the opening of the by-pass valve. A stripping pump (not shown in Figure A-2), in series with the by-pass valve, is used to produce very low pressures. The vacuum pump is used to remove air from the system so as to keep it full of water at all times.

The energy put into the water of the main circuit by the circulating pump (up to 250 HP) is all dissipated in heat. To prevent the temperature of the water from rising to undesirable values, it is necessary to remove this heat by cooling. Part of the water returned through the by-pass valve is picked up by the cooling water pump, circulated through the forced-draft cooling tower on the roof, and returned to the sump. By varying the quantity of water circulated through the cooling system, it is possible to maintain the water in the main circuit at a constant temperature.

BALANCE

The balance, shown schematically in Figure A-3, is designed to measure three components of the hydrodynamic forces acting on the model. These are the drag force parallel to the flow, the cross force normal to the flow, and the moment around the axis of support. The three forces to be measured are transmitted hydrostatically to three self-balancing, weighing type pressure gages. These automatic gages, under glass covers, may be seen in Figure A-4, which is a view of the operating floor of the Water Tunnel. The fourth gage shown in this figure is a weighing type manometer used to determine the velocity in the working section by measuring the pressure drop across the reducing nozzle. The gages are responsive to a change in the drag or cross force acting on the model of 0.02 pounds, and a change of 0.04 inch-pounds in the moment.

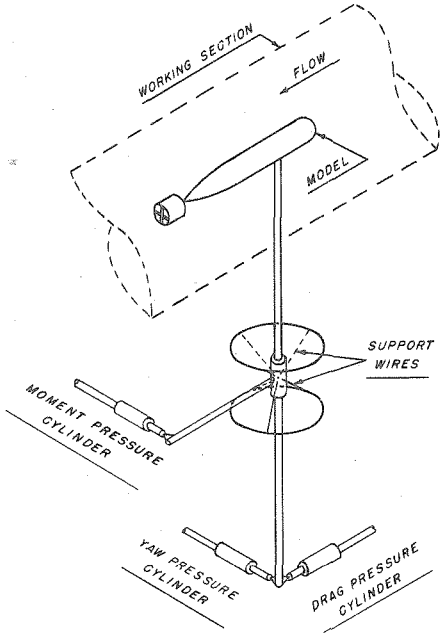


FIGURE A-3

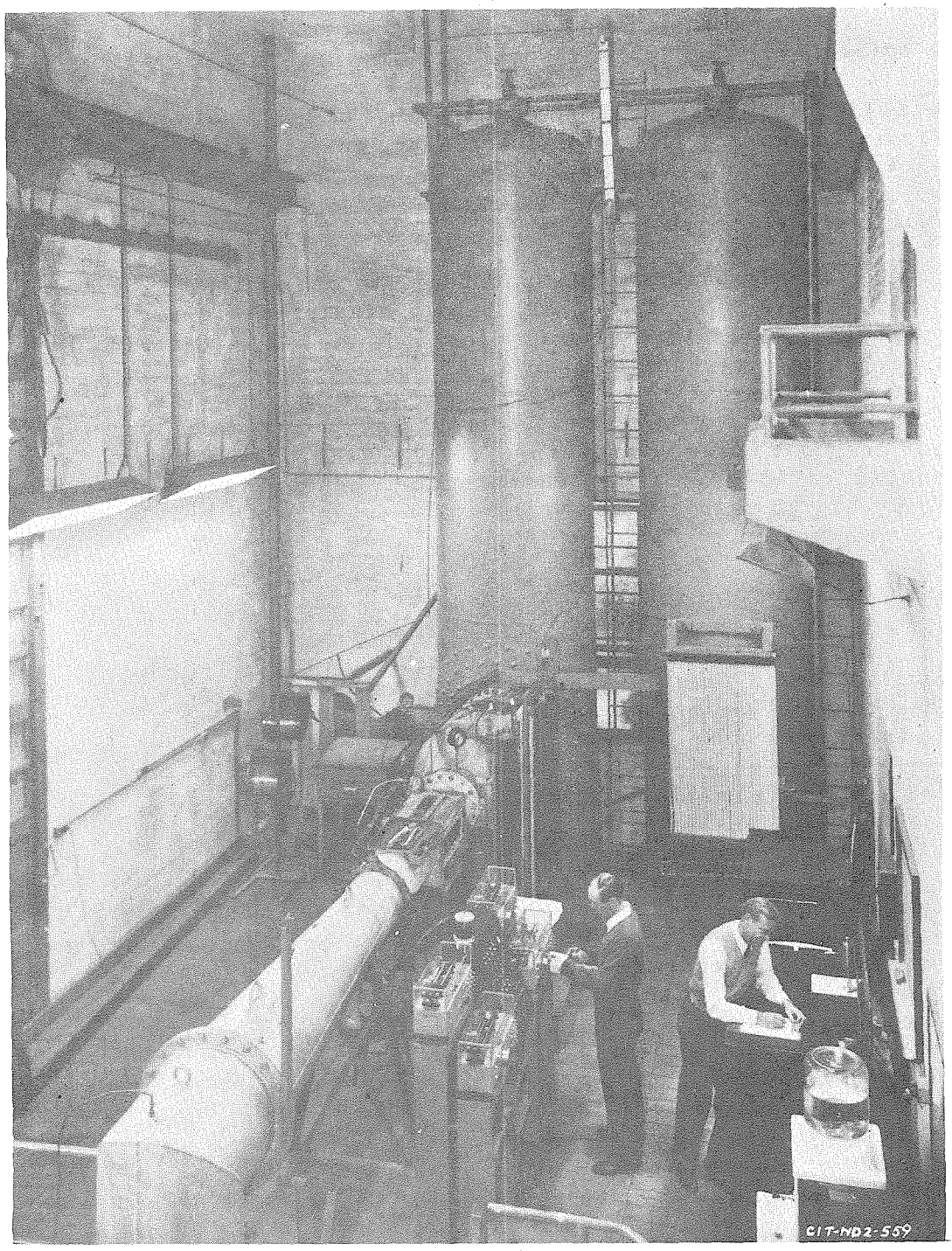


FIGURE A-4

OPERATING FLOOR

OF THE

HIGH SPEED WATER TUNNEL

HYDROFOIL TEST INSTALLATION

The arrangement of the Water Tunnel working section used for these hydrofoil tests is shown in Figure A-5. Two parallel walls were installed 10" apart at top and bottom of the 14" diameter working section. A smooth transition was made at each end of the walls from the circular to the approximately rectangular cross section. By locating the hydrofoil test section spanwise between the two walls, two-dimensional flow conditions could be approximated. The test span was supported at one tip by the balance spindle as shown and cantilevered into the stream. By rotating the spindle the hydrofoil angle of attack was changed. Measurements of drag, lift, and pitching moment were obtained as reactions at the drag, yaw, and moment pressure cylinders shown in Figure A-3.

Two variations of the two-dimentional installation were used. In one the hydrofoil unit spanned the entire 10" depth between the top and bottom walls except for small clearance gaps at either wall. The test span had a chord of 3", making the aspect ratio equal 3.33. This is the arrangement shown at the left in Figure A-6. In selecting the proportions of the hydrofoil test unit two things were taken into account. The first was the physical capacity of the balance (200 lb lift), and the second was the structural rigidity of the hydrofoil unit itself. In order to come within the capacity range of the balance it was necessary to reduce the size and hence the thickness and rigidity of the cantilevered hydrofoil in the lift direction so much that at high lifts rather severe deflections occured if the full 10" span were used. Consequently, for the second installation shown at the right in Figure A-6, the test unit spanned only one-half of the 10" gap, extending from the bottom wall to the tunnel center line and a dummy hydrofoil section was extended from the top down to the center line to complete the remaining half span. With this set-up the balance measured only one-half the forces and moments on the total 10" section and the range of the experiments could be extended to higher velocities and lifts than were possible with the complete 10" span. A small gap at the lower wall and at the center line of the tunnel between the ends of the two semispans provided the clearance necessary for isolation of the two spans. An angle indexing device was provided to change the pitch angle of the upper section simultaneously with the lower half span.

Figure A-7 is a side view of the working section and tunnel balance showing the upper semispan in position and the bottom half mounted on the Water Tunnel balance ready to be lifted into position for testing. Figure A-8 is a close-up view of the lower semispan and balance assembly. The circular disc forms part of the lower parallel wall and is separated from the hydrofoil by a small clearance. Figure A-9 is a view looking downstream into the tunnel working section with the parallel walls and the hydrofoil test unit in place.

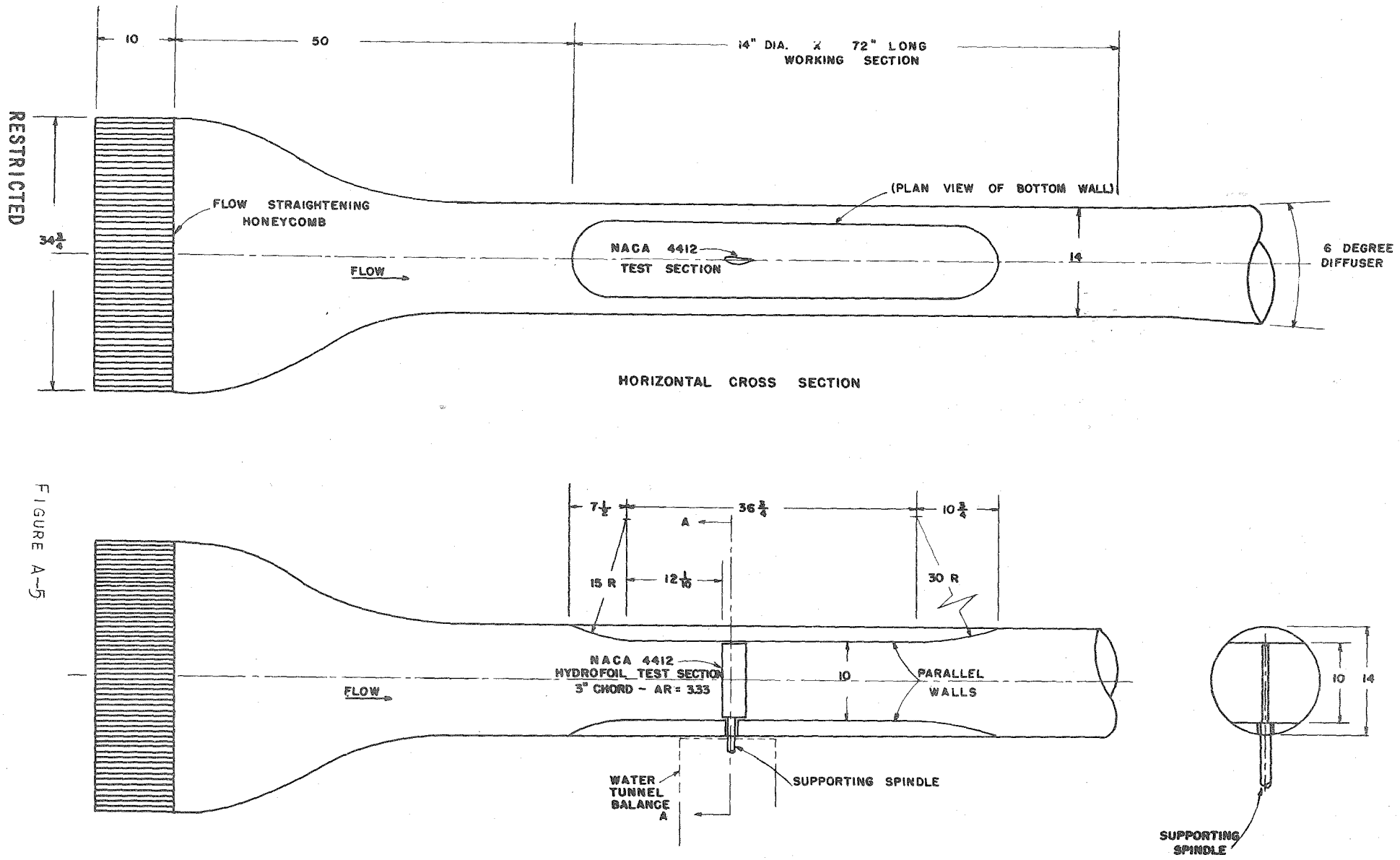


ND- 795-7

FIGURE A-5

# HYDROFOIL TEST INSTALLATION



RESTRICTED

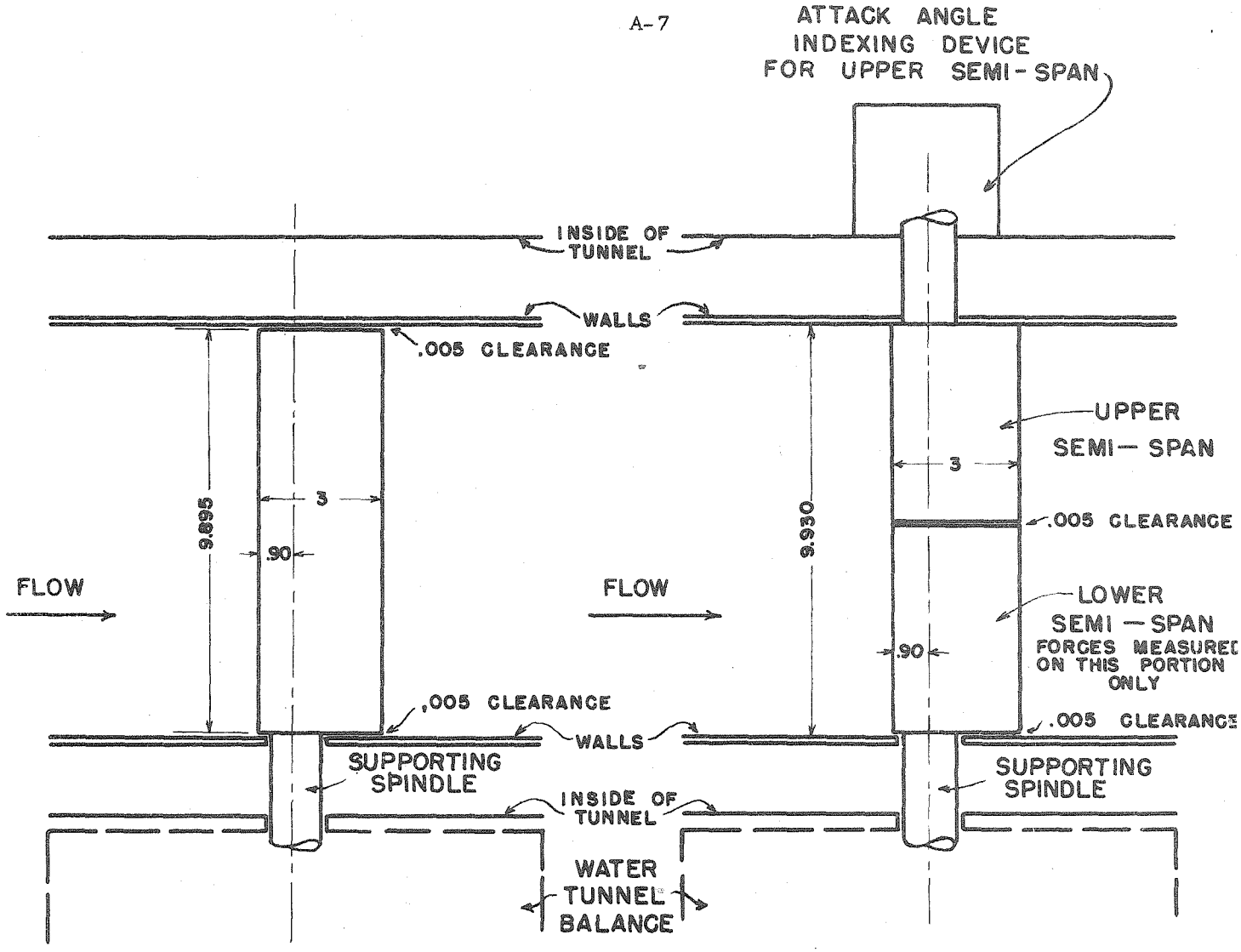


## DETAILS OF TEST INSTALLATIONS

## WITH SPLIT SPAN AND FULL SPAN HYDROFOIL UNITS

FIGURE A-6

DRG. ND-810-T

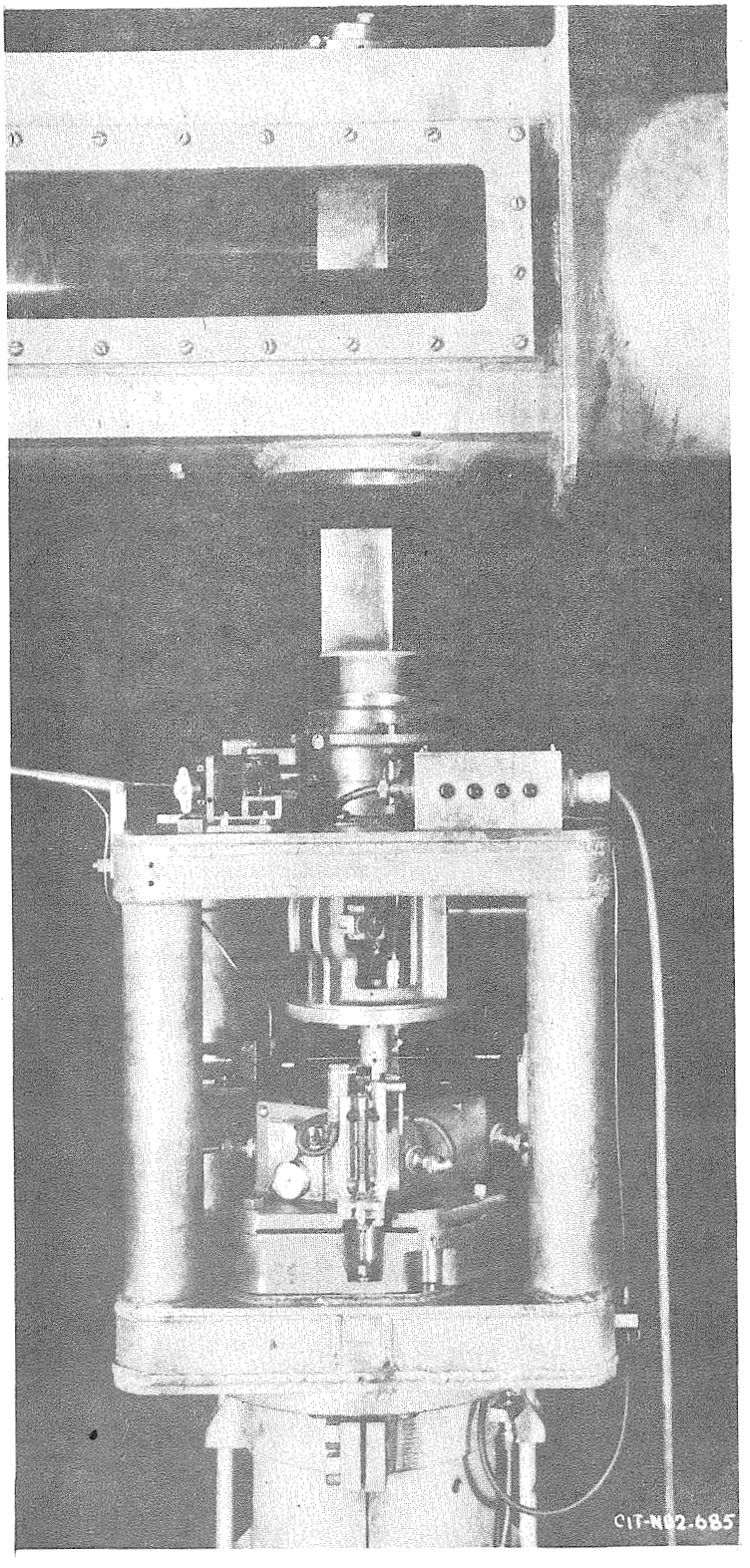


FIGURE A-7

SIDE VIEW OF WATER TUNNEL INSTALLATION SHOWING UPPER SEMISPAN IN PLACE IN WORKING SECTION AND LOWER SEMISPAN ATTACHED TO BALANCE. INSTALLATION IS COMPLETED BY RAISING BALANCE AND PROJECTING LOWER SPAN INTO WORKING SECTION TO MEET UPPER SPAN.

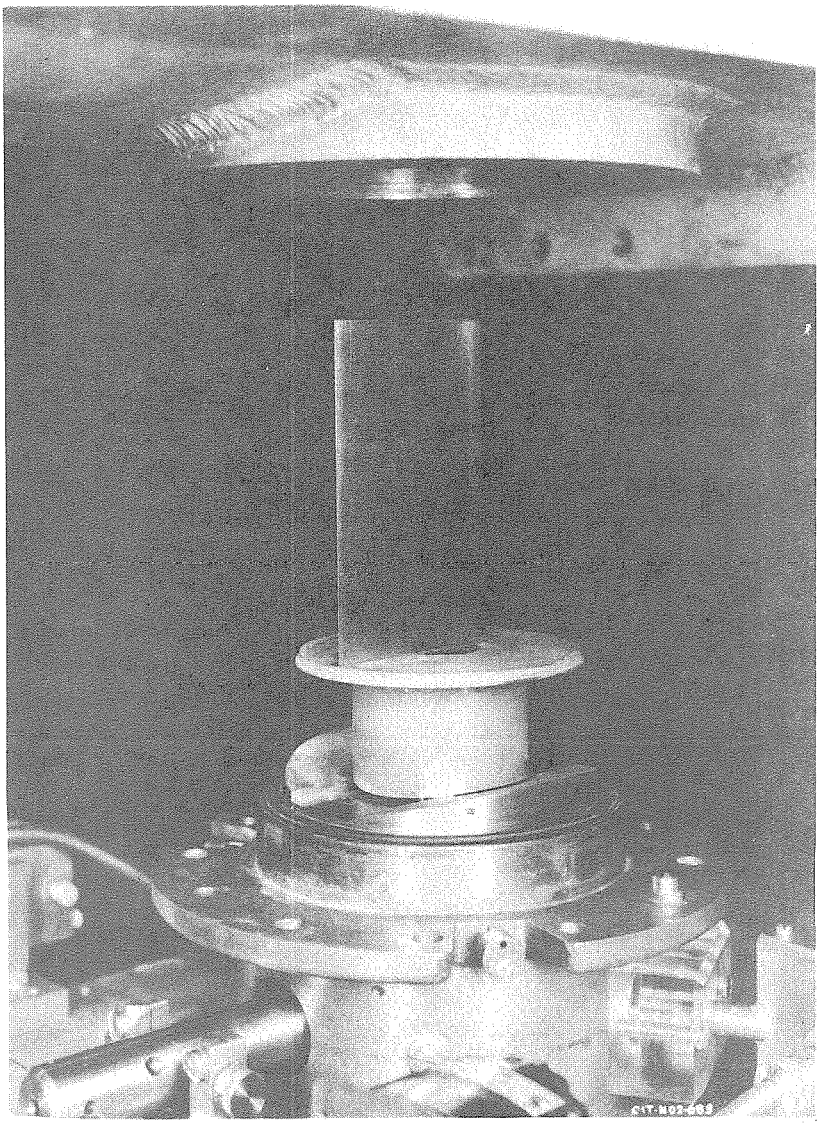

FIGURE A-8

DETAILS OF HYDROFOIL MOUNTING ON BALANCE. CIRCULAR DISC SHOWN FORMS A PART OF THE LOWER PARALLEL WALL AND IS SEPARATED FROM THE HYDROFOIL BY A SMALL CLEARANCE.

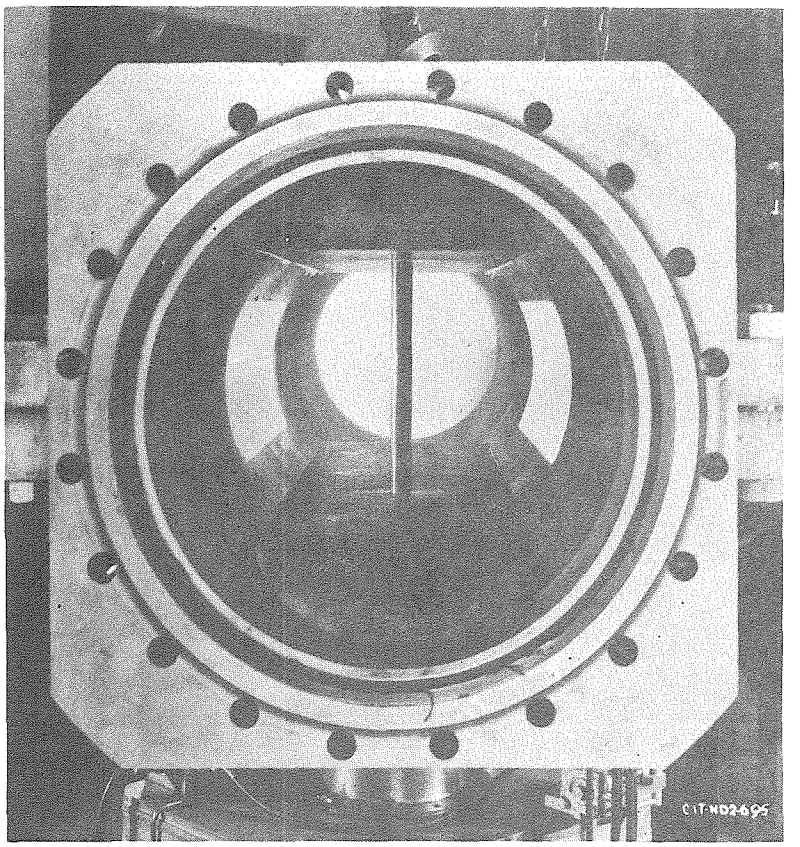


FIGURE A-9

VIEW LOOKING DOWNSTREAM INTO TUNNEL WORKING SECTION WITH THE PARALLEL WALLS AND HYDRO-FOIL TEST SPAN IN PLACE.

TEST PROCEDURES

The facilities of the High Speed Water Tunnel provide for great flexibility in operation and test procedures. Individual test runs are usually made to determine the effect of the hydrodynamic forces of individual variables, although any of the variables may be changed at will independently of the others. Because of the two-dimensional character of the hydrofoil installation, a single test covering the desired range of pitch angles was sufficient to determine the hydrodynamic characteristics of the hydrofoil at any given velocity.

Variable speed test runs are necessary if the scale (Reynolds number) effect on the hydrodynamic forces is to be determined. The speed can be varied in as many steps as desired and the forces measured at each step. During these tests the pressure in the working section is kept high enough to suppress cavitation at the highest velocity.

In order to determine cavitation characteristics, tests are made during which the pressure is varied while all other factors are held constant. The inception and development of cavitation is observed and photographed through the transparent windows of the working section. Simultaneously velocity and pressure measurements are made from which values of the cavitation parameter can be calculated. If the cavitation does not make the test model dynamically unstable and cause it to vibrate, the hydrodynamic forces and moments can also be measured. These tests can be repeated at as many velocities as desired.

The photographs of cavitation included in the report are flash pictures taken with lamps having a flash duration of about 20 microseconds.

# APPENDIX B

## DEFINITIONS OF TERMS AND SYMBOLS

$\alpha_o$ = angle of attack between hydrofoil mean flow of water in degrees

$d_o$ = drag force per unit length of hydrofoil span in pounds

$l_o$ = lift force per unit length of hydrofoil span in pounds

$m_{a.c.}$ = pitching moment per unit length of hydrofoil span in foot pounds, measured about the aerodynamic center

V = relative velocity between the water and the hydrofoil in feet per second

$\rho$ = density of water in slugs per cubic foot

$\mu$ = absolute viscosity of water in pound seconds per square foot

c = chord of hydrofoil section in feet

b = span of hydrofoil test unit in feet

b/c = aspect ratio

a.c. = aerodynamic center, the point about which the pitching moment coefficient is independent of lift

C.P. = center of pressure, the point at which the resultant of all the hydrodynamic forces acting on the hydrofoil is applied

Section Drag Coefficient

$$c_{d_o} = \frac{d_o}{\rho \frac{V^2}{2} c}$$

Section Lift Coefficient

$$c_{l_o} = \frac{l_o}{\rho \frac{V^2}{2} c}$$

Section Moment Coefficient (about aerodynamic center)

$$c_{m_{a.c.}} = \frac{m_{a.c.}}{\rho \frac{V^2}{2} c^2}$$

Reynolds Number

$$R = \frac{Vc\rho}{\mu}$$

# APPENDIX C

The 4412 hydrofoil shape is the same as the NACA 4412 Airfoil shape described in References (9), (4), (5), and (6). Dimensions of the profile are tabulated in Figure C-1. For these experiments solid stainless steel test sections with a chord length of 3" were supplied the laboratory by the David Taylor Model Basin. Photographs of the test units are shown in Figures 1, 2, and 3 of this report. Details of the test installations are given in Appendix A.

| Station | Upper | Lower | Station | Upper | Lower |
|---|---|---|---|---|---|
| 0 | — | 0 | 40 | 9.80 | -1.80 |
| 1.25 | 2.44 | -1.43 | 50 | 9.19 | -1.40 |
| 2.5 | 3.39 | -1.95 | 60 | 8.14 | -1.00 |
| 5.0 | 4.73 | -2.49 | 70 | 6.69 | -0.65 |
| 7.5 | 5.76 | -2.74 | 80 | 4.89 | -0.39 |
| 10 | 6.59 | -2.86 | 90 | 2.71 | -0.22 |
| 15 | 7.89 | -2.88 | 95 | 1.47 | -0.16 |
| 20 | 8.80 | -2.74 | 100 | 0.13 | -0.13 |
| 25 | 9.41 | -2.50 | 100 | — | 0 |
| 30 | 9.76 | -2.26 | | | |

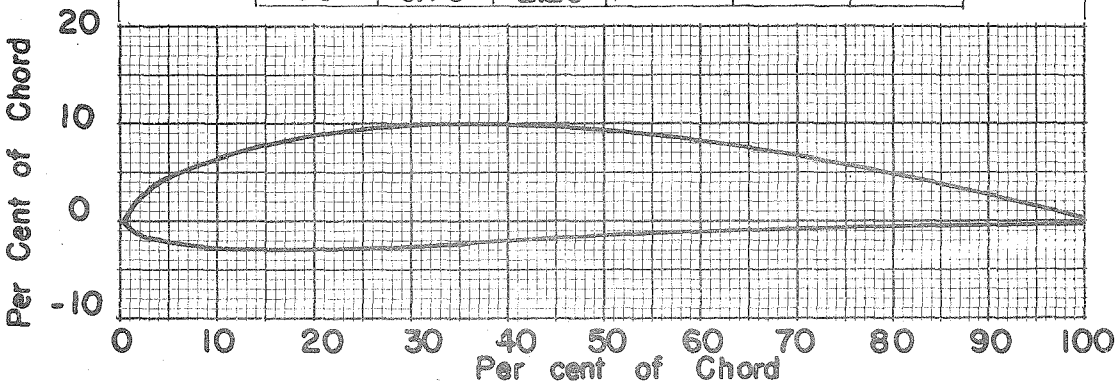


## N. A. C. A. 4412 AIRFOIL

Leading Edge Radius 1.58

Slope of Radius through End of Chord 4/20

MAXIMUM MEAN CAMBER = 0.04 X CHORD

LOCATION OF MAX. CAMBER = 0.4 X CHORD

MAXIMUM THICKNESS = 0.12 X CHORD

REF. NACA TECH. REP. 460 ND — 794 — T

Cavitation Parameter

$$K = \frac{P_L - P_b}{\rho \frac{V^2}{2}}$$

Where in addition to terms defined above

$P_L$ = absolute pressure in the undisturbed flow in pounds per square foot

$P_b$ = pressure in the cavitation bubble (taken as equal to the vapor pressure of water for these tests) in pounds per square foot

# APPENDIX D

## REFERENCES

(1) "The High Speed Water Tunnel at the California Institute of of Technology," by R. T. Knapp, V. A. Vanoni, and J. W. Daily, HML Rep. ND-1, June 29, 1942

(2) "The Characteristics of 78 Related Airfoil Sections from Tests in the Variable Density Wind Tunnel," by E. N. Jacobs, K. E. Ward, and R. M. Pinkerton, NACA T. R. No. 460, 1933

(3) "Calculated and Measured Pressure Distributions over the Midspan Section of the NACA 4412 Airfoil," by R. M. Pinkerton, NACA T. R. No. 563, 1936

(4) "Airfoil Section Characteristics as Affected by Variations of the Reynolds Number," by E. N. Jacobs, and A. Sherman, NACA T. R. No. 586, 1937

(5) "Airfoil Section Data Obtained in the NACA Variable-Density Tunnel as Affected by Support Interference and Other Corrections," by E. N. Jacobs and I. H. Abbot, NACA T. R. No. 669, 1939

(6) "Aerodynamics of the Airplane," by C. B. Millikan, Wiley, 1941

(7) "Aerodynamic Theory," Vol. II, edited by W. F. Durand, Julius Springer (Berlin), 1934

(8) "Determination of the Characteristics of Tapered Wings," by R. F. Anderson, NACA T. R. No. 572, 1936

(9) "The Design of Propeller Pumps and Fans," by M. P. O'Brien and R. G. Folsom, Univ. of Calif. Publ. in Engr. Vol4, No. 1, University of Calif. Press, 1939

(10) See Confidential report on high frequency sound measurements by R. T. Knapp, HML Rep. ND-8.2, Section No. 6.1-sr207-924, August 31, 1943